Incorporation of multi-phase halogen chemistry into Community Multiscale Air Quality (CMAQ) model

Kiyeon Kim[1], Chul Han Song[1]*, Kyung Man Han[1], Greg Yarwood[2], Ross Beardsley[2], and Saewung Kim[3]

1. School of Earth Science and Environmental Engineering, Gwangju Institute of Science and Technology (GIST), Gwangju 61005, Republic of Korea
2. Ramboll, Novato, CA 94945, USA
3. Department of Earth System Science, University of California, Irvine, CA, USA

Shortened title: Multi-phase halogen chemistry

*Corresponding author: Chul Han Song (chsong@gist.ac.kr)

Abstract

~~Recent studies have revealed that h~~Halogen radicals (Cl, Br, and I) significantly influence atmospheric oxidation capacity, affecting <u>both</u> O_3 formation ~~or~~ <u>and</u> destruction. However, understanding of halogen ~~chemistries~~ <u>chemistry</u> remains limited. To better investigate <u>comprehensive</u> atmospheric halogen ~~chemistries~~<u>chemistry</u>, we incorporated halogen processes into the Community Multi-scale Air Quality (CMAQ) model: (i) emissions of Cl_2, HCl, Br_2, and HBr from anthropogenic sources, and Br_2, I_2, HOI, and halocarbons from natural sources; and (ii) 177 multi-phase halogen reactions. ~~After developing the model, we examined its performance against observed data. The results demonstrated significant improvements in simulating observed nitryl chloride ($ClNO_2$) mixing ratios at supersites. The index of agreement (IOA) improved from 0.41 to 0.66, and the mean bias (MB) decreased from −159.36 ppt to −25.07 ppt. These improvements were driven by four atmospheric key reactions: (i) $ClO + ClO \rightarrow Cl_2$; (ii) $HOBr + Cl^- \rightarrow BrCl$; (iii) different parameterization of γ_{N2O5}; and (iv) $2NO_2 + Cl^- \rightarrow ClNO + NO_3^-$. We then examined the~~ <u>Model performance was evaluated against observed $ClNO_2$ levels, and by comparison with reported ranges of BrO and IO levels. The updated model showed significant improvements in simulating $ClNO_2$ mixing ratios, with the index of agreement (IOA) increasing from 0.41 to 0.66 and mean bias (MB) decreasing from −159.36 ppt to -25.07 ppt at supersites. Furthermore, simulated BrO and IO levels fell within the ranges reported in previous studies. We found that these improvements were driven by four key reactions: (i) ClO self-reaction, (ii) heterogeneous HOBr chemistry, (iii) NO_2 uptake, and (iv) revised N_2O_5 parameterization. Based on our modeling system, we found that the presence of halogen radicals led to changes in the</u> net O_x production rate ($P(O_x)$), which increased from 3.08 ppb/h to 3.33 ppb/h on land and decreased from 0.21 ppb/h to 0.07 ppb/h over ocean<u>.</u> ~~in the presence of halogen radicals.~~ <u>It was noted that</u> ~~Further analysis of the impacts of halogen processes on key atmospheric species revealed that~~ levels of OH, HCHO, and NO_x

2

48 also increased by ~0.007 ppt (5.5%), ~0.03 ppb (1.6%), and ~0.29 ppb (2.9%), respectively,

49 while levels of HO$_2$ and VOCs decreased by ~0.45 ppt (5.3%) and ~0.71 ppb (5.9%).

50 respectively. These results highlight the importance of accurately representing halogen

51 processes in regional air quality models.

52

53

3

1. Introduction

Atmospheric oxidants, such as OH, NO_3, and O_3, play a significant role in atmospheric chemistry. These oxidants react with volatile organic compounds (VOCs), leading to the formation of peroxyl radicals (RO_2), which, in turn, influences the O_3 formation. They also contribute to the formation of secondary organic and inorganic aerosols. Meanwhile, halogen radicals (such as Cl, Br, and I) also serve as oxidants in the atmosphere, affecting the oxidation capacity through various reactions (R1 – R4; see below) (Simpson et al., 2015; von Glasow and Crutzen, 2003; Fan and Li, 2022).

$$X \text{ (Cl, Br, and I)} + VOC \rightarrow RO_2 \tag{R1}$$

$$RO_2 + NO \rightarrow NO_2 + RO \tag{R2}$$

$$HO_2 + NO \rightarrow NO_2 + OH \tag{R3}$$

$$NO_2 \overset{hv}{\rightarrow} O^{3p} + O_2 \overset{M}{\rightarrow} O_3 \tag{R4}$$

$$X + O_3 \rightarrow XO + O_2 \tag{R5}$$

$$XO + HO_2 \rightarrow HOX + O_2 \tag{R6}$$

$$HOX \overset{hv}{\rightarrow} X + OH \tag{R7}$$

These radicals can also make substantial impacts on the O_3 loss via reactions (R5) – (R7) (Saiz-Lopez et al., 2012; Sarwar et al., 2015; Simpson et al., 2015). Given their roles in both the O_3 formation and destruction, a comprehensive understanding of atmospheric halogen ~~chemistries~~ chemistry is essential for accurately assessing the oxidative potentials of the atmosphere.

In this context, several studies attempted to incorporate chlorine chemistry into chemical-transport models (e.g., Yi et al., 2021; Sarwar et al., 2012; Qiu et al., 2019a and b). Specifically, Qiu et al. (2019a) reported that heterogeneous reactions involving reactive chlorine species can increase O_3 levels by approximately 20%. Moreover, Liu et al. (2018) found that the mixing ratios of O_3 increased by ~7.7 ppbv when anthropogenic chlorine emissions were included.

4

82   On the other hand, numerous studies have emphasized not only the significance of

83 chlorine chemistry but also the influences of the synergistic effects of bromine and iodine

84 chemistry with chlorine chemistry (Sarwar et al., 2019; Simpson et al., 2015; Caram et al.,

85 2023; Badia et al., 2019; Saiz-Lopez et al., 2014; Li et al., 2022; Iglesias-Suarez et al., 2020).

86 For instance, modeling studies considering both bromine and iodine chemistries showed that

87 simulated O_3 levels actually decreased by 15.9 ppb (Parrella et al., 2012; Sarwar et al., 2015;

88 Herrmann et al., 2022; Gantt et al., 2017; Read et al., 2008; Huang et al., 2021). These findings

89 strongly suggest that incorporating chlorine processes, together with bromine and iodine

90 processes, is crucial for correct and comprehensive understanding of atmospheric chemistry.

91   The Korean Peninsula, surrounded by the Yellow Sea, Korea Strait, and the East Sea,

92 is characterized by high population density and highly industrial regions. Therefore, it can be

93 influenced by both natural (oceanic) and anthropogenic halogen emissions. However, almost

94 no modeling study has taken into account the natural and anthropogenic halogen processes

95 over/around South Korea. Although almost no research has been carried out to examines the

96 impacts of halogen chemistry on atmospheric composition over/around South Korea, several

97 studies have considered atmospheric chlorine processes using 3D chemical-transport models

98 (CTMs) (e.g., Jo et al., 2023; Kim et al., 2023). Given the synergistic effects of chlorine,

99 bromine and iodine chemistries in the atmosphere, a comprehensive study that takes all these

100 halogen processes into account is absolutely necessary.

101   For the comprehensive analysis of halogen processes and their influence on regional

102 air quality, we established anthropogenic and natural halogen emissions and incorporated full

103 sets of halogen reactions into the framework of the Community Multi-scale Air Quality

104 (CMAQ) model. Specifically, we incorporated the following halogen processes into the CMAQ

105 model: (i) atmospheric chlorine processes (anthropogenic HCl and Cl_2 emissions with 58

106 chlorine reactions); (ii) atmospheric bromine processes (anthropogenic and natural HBr and

107 Br$_2$ emissions together with 64 bromine reactions); and (iii) atmospheric iodine processes (HOI

108 and I$_2$ natural emissions, along with 55 iodine reactions). ~~The primary objective of this study is~~

109 ~~to develop improved atmospheric halogen processes with updated (modified) halogen~~

110 ~~chemistry. We then investigate the formation of ozone using the new halogen processes, also~~

111 ~~exploring the impacts of the halogen radicals on the mixing ratios of the key atmospheric~~

112 ~~species such as OH, HO$_2$, HCHO, VOC$_s$, and NO$_x$.~~

113 Based on this modeling system, the primary objectives of this study are threefold: (i)

114 to develop and implement an updated halogen chemistry that accounts for the interactions

115 among multiple halogen species; (ii) to evaluate model performance using observational data

116 from the Korea US Air Quality (KORUS-AQ) campaign (1 May – 12 June, 2016), including

117 direct ClNO$_2$ measurements and inferred estimates of BrO and IO; and (iii) to examine the

118 atmospheric impacts of the updated halogen chemistry on a broader set of key atmospheric

119 constituents such as O$_3$, OH, HO$_2$, HCHO, VOC$_s$, and NO$_x$. In this context, this study is

120 designed to support a comprehensive understanding of atmospheric halogen processes and their

121 implications for regional air quality. ~~To achieve these research goals, we incorporated the~~

122 ~~following halogen processes into the CMAQ model: (i) atmospheric chlorine processes~~

123 ~~(anthropogenic HCl and Cl$_2$ emissions with 58 chlorine reactions); (ii) atmospheric bromine~~

124 ~~processes (anthropogenic and natural HBr and Br$_2$ emissions together with 64 bromine~~

125 ~~reactions); and (iii) atmospheric iodine processes (HOI and I$_2$ natural emissions, along with 55~~

126 ~~iodine reactions). After these works, we evaluated the performances of the modified CMAQ~~

127 ~~model against field observations obtained from the Korea US Air Quality (KORUS-AQ)~~

128 ~~campaign (May – June, 2016).~~

129

130 **2. Methodology**

131   In this study, we incorporated homogeneous, aqueous, and heterogeneous halogen

132   reactions into the CMAQ model, along with emissions of halogen species. To evaluate the

133   accuracy of these halogen processes, we compared the model results with observational data

134   from the KORUS-AQ campaign (Jeong et al., 2019; Crawford et al., 2021). This section

135   provides several details on the observation data, the WRF-CMAQ model configurations, and

136   the atmospheric halogen processes, including halogen reactions and emissions.

137   **2.1 Observation data**

138   Mixing ratios of nitryl chloride ($ClNO_2$) were measured every five minutes at Olympic

139   Park (37.52°N; 127.12°E) and Mt. Taewha (37.27°N; 127.41°E) stations during the period of

140   the KORUS-AQ campaign (refer to two blue stars in Fig. 1a), using Chemical Ionization Mass

141   Spectrometer (CIMS). The CIMS instrument has a detection limit of 1.5ppt and an uncertainty

142   within 20%. Further details on the CIMS instrument are found in Slusher et al. (2004) and

143   Jeong et al. (2019). In our study, $ClNO_2$ observations were utilized to evaluate the performances

144   of the modified CMAQ model simulations. These results are discussed in Sect. 3.1.

145   **2.2 WRF-CMAQ model description**

146   The Weather Research and Forecasting (WRF) v3.8.1 model simulations were carried

147   out to generate meteorological fields (Skamarock et al., 2008). The details of physical

148   parameters used in the WRF simulations are summarized in Table S1. National Center for

149   Environmental Prediction Final Analysis (NCEP-FNL) data were used for initial and boundary

150   conditions. The WRF model included a 5-day spin-up period to minimize uncertainties from

151   the initial and boundary conditions.

152   This study also included the CMAQ v5.2.1 model simulations (Byun and Schere, 2006)

153   over a domain covering northeast Asia with 273×204 horizontal grid cells. The grid

154   resolution is 15×15 km^2 with 15 vertical layers from surface to 50 hPa. The Statewide Air

155   Pollution Research Center-07 (SAPRC-07TC) mechanism (Carter, 2010; Hutzell et al., 2012)

with AERO6 module was used in the CMAQ model simulations. One limitation of the SAPRC-07TC mechanism is that it has only basic chlorine chemistry. In order to implement more sophisticated halogen model simulations, we incorporated additional and updated halogen reactions into the SAPRC-07TC mechanism. The detailed reactions are explained in Sects. 2.4.1 and 2.4.2.

In order to ~~derive~~ run the CMAQ model, biomass burning and biogenic emissions were obtained from the Fire Inventory from NCAR (FINN) v1.5 (Wiedinmyer et al., 2011) and the Model of Emissions of Gases and Aerosol from Nature (MEGAN) v2.1 (Guenther et al., 2012), respectively. Anthropogenic emissions were acquired from the KORUS v5.0 emission inventory (Woo et al., 2020), specifically developed for the KORUS-AQ campaign. The KORUS v5.0 inventory covers emissions of primary pollutants such as NO_x, CO, HCHO, VOCs, and particulate chlorine (pCl^-), but it omits the emissions for anthropogenic chlorine species (HCl and Cl_2), bromine species (HBr and Br_2), and ocean-generated halogen species (HOI, I_2, and halocarbons). We have thus developed new halogen emissions for this study. The methodology for developing the halogen emissions will be discussed in Sections 2.3.1 and 2.3.2.

2.3 Halogen emissions

In this section, we discuss the development of anthropogenic and natural halogen emissions within our model framework.

2.3.1 Anthropogenic emissions

First, we assumed that emissions of anthropogenic HCl and Cl_2 ~~are~~ mainly originated from coal combustion. Coal combustion occurs predominantly in four main sectors: industry, residential areas, power plants, and other sectors such as agriculture and furniture manufacturing. In addition, HCl emissions ~~are~~ also ~~taking~~ take place from municipal solid waste incineration.

8

181 To calculate chlorine emissions from industry and residential areas, we utilized coal

182 consumption data from the 2016 Regional Energy Report of South Korea

183 (https://www.keei.re.kr). Thereafter, the emissions of HCl and Cl_2 from these sectors were

184 calculated using the following equation (1):

185 $$E_{i,j} = M_{i,j} \times EF_{i,j} \times \rho \times \frac{1}{MM} \times \frac{1}{10^3} \qquad\qquad \text{(Eq. 1)}$$

186 where, $E_{i,j}$ represents the emission for species i in categories j (Mg); M denotes the coal

187 consumption (Gg); and EF is the emission factor ($\mu g/g$) calculated using the method from a

188 previous study (Jiang et al., 2005 (in Chinese)). ρ indicates the percentage of HCl and Cl_2 in

189 the chlorine content of coal. In our study, percentages of 86.3% and 3.63% for ρ_{HCl} and ρ_{Cl2}

190 were used, respectively, based on research conducted by Deng et al. (2014) and Liu et al. (2018).

191 MM represents the ratios of the molar mass of the chlorine atom to the molecular weight (i.e.,

192 35.5/36.5 for HCl and 1 for Cl_2).

193 For the remaining three sectors, namely power plants, solid waste incineration, and

194 others, the HCl emissions were obtained directly from the Korean tele-monitoring system

195 (TMS) named the CleanSYS (https://cleansys.or.kr). Meanwhile, the emissions of Cl_2 from

196 these sectors can also be calculated using equation (1), based on the HCl emissions previously

197 calculated.

198 Bromine emissions (HBr and Br_2) were additionally estimated from the previously

199 calculated chlorine emissions. According to a recent study, bromine is also emitted from the

200 coal combustion with a ratio (0.25) of bromine to chlorine concentrations (Peng and Wu, 2014).

201 These bromine emissions were split~~ted~~ into 70% and 30% for HBr and Br_2, respectively. The

202 detailed methodology used in our study is summarized in Li et al. (2021).

203 Consequently, we developed an emission inventory that includes anthropogenic

204 chlorine and bromine emissions. Figure 1 illustrates the spatial distributions of these emissions

205 across South Korea. The total emission rates for anthropogenic HCl, Cl_2, HBr, and Br_2 in South

9

206 Korea are 5,989.6, 450.8, 460.8, and 240.8 Mg·yr^{-1} respectively. These values are higher than

207 those reported in previous studies conducted for the same region and time period. For instance,

208 Jo et al. (2023) estimated that total anthropogenic HCl emissions were less than 1.0 Gg,

209 whereas Kim et al. (2023) reported a value of 1.35Gg. In contrast, Kim et al. (2023) reported

210 smaller emission fluxes for HCl over the same region. These discrepancies may result from the

211 inclusion of additional HCl emissions from the residential and industrial sectors in our study.

212 Moreover, our research also accounts for emissions of Cl_2, HBr, and Br_2. It is noteworthy that

213 Cl_2, HBr, and Br_2 have relatively shorter e-folding lifetimes (a few minutes for Cl_2 and Br_2,

214 and a-few hours for HBr) than HCl (about 1.5 days), which may increase the oxidant capacity

215 in the atmosphere.
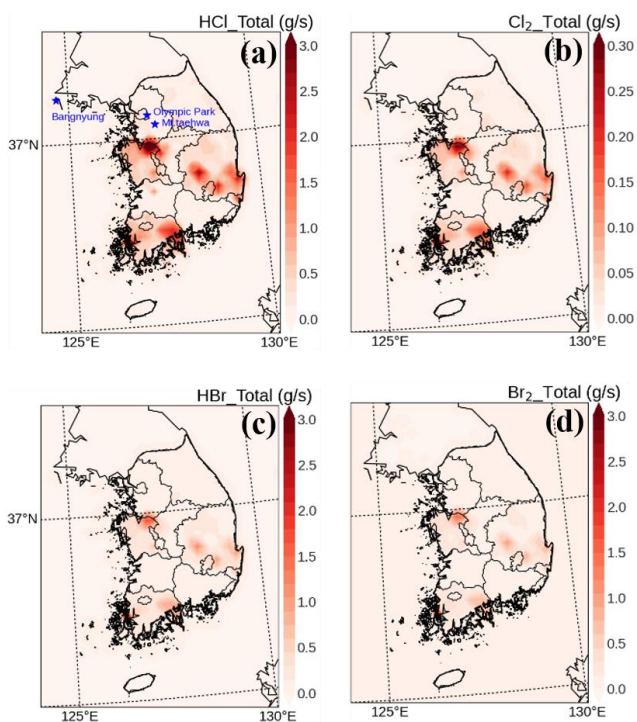
Figure 1. Spatial distributions of anthropogenic emission rates of (a) HCl, (b) Cl_2, (c) HBr, and (d) Br_2 during the period of the KORUS-AQ campaign over South Korea. Three blue stars denote the locations of three supersites (Bangnyung, Olympic Park, and Mt. Taehwa) during the KORUS-AQ campaign.

2.3.2 Natural emissions

Biogenic halocarbons, such as $CHBr_3$, CH_2Br_2, $CHBrCl_2$, CH_2BrCl, $CHBr_2Cl$, CH_2I_2, CH_3I, CH_2ICl, and CH_2IBr, are emitted from micro-algae activities in the ocean. To calculate these emissions of bromine and iodine-containing halocarbon species, we used the chlorophyll-a (chl-a) concentrations as a proxy for the photosynthetic activity of phytoplankton (Liss et al., 2014).

Chlorophyll-a concentrations in the ocean have been monitored by various satellite sensors such as Moderate Resolution Imaging Spectroradiometer (MODIS) and Geostationary Ocean Color Imager (GOCI) (Kim et al., 2016; O'reilly and Werdell, 2019; Sarwar et al., 2015).

11

231   Among these sensors, Park et al. (2015) reported that the chlorophyll-a concentrations

232   measured by the GOCI sensor showed the best agreements with surface observations compared

233   to those from the MODIS sensor in the East Asian ocean. Based on this study, we applied the

234   chlorophyll-a data from the GOCI sensor into our study (refer to Fig. S1).

235   Gridded halocarbon emissions were estimated using the following equation (2)

236   (Sarwar et al., 2015):

237         $E_{Halocarbon} = 1.2 \times 10^{-11} \times (O_F + S_F) \times A_{GC} \times f_{HC} \times f_{DP} \times [chl\text{-}a]$ (Eq.2)

238   where, O_F and S_F represent the ocean and coastal fractions of the grid cell, respectively. A_{GC}

239   denotes the area of the grid cell (m^2). f_{HC} is the emission factor for the species; and f_{DP}

240   represents the diurnal profile. [$chl\text{-}a$] ~~means~~ denotes the chlorophyll-a concentration. The

241   distributions of natural bromine and iodine emissions are shown in Fig. S2.

242   Natural Br$_2$ emissions were estimated by debromination of sea-salt aerosols (SSAs),

243   following the method proposed by Sarwar et al. (2015) and Yang et al. (2005). In this approach,

244   Br$^-$ contained within the SSAs was released into the atmosphere as Br$_2$ (i.e., dehalogenation of

245   SSAs). This process was parameterized based on sea-salt aerosol mass, Br/NaCl mass ratio,

246   sea surface temperature, and 10-m wind speed. ~~which were derived using the mass ratios of Br~~

247   ~~to NaCl within SSAs.~~ In addition, inorganic iodine (such as HOI and I$_2$) emissions were

248   calculated at the air-sea water interfaces, utilizing information on dry deposition of O$_3$ over the

249   ocean. This approach is based on the fact that the formations of HOI and I$_2$ are initiated by

250   reaction between iodide (I$^-$(aq)) and O$_3$ at the ocean surfaces. ~~Sarwar et al. (2015) employed~~

251   ~~the same methodology for developing these emissions. The distributions of natural bromine~~

252   ~~and iodine emissions are shown in Fig. S2.~~ More detailed information on natural inorganic

253   emissions can be found in Sarwar et al. (2015).

254   **2.4 Halogen chemical reactions**

As mentioned previously, the conventional CMAQ v5.2.1 model accounts for only a limited set of chlorine-related processes: (i) reactions between VOCs and Cl radicals (Sander et al., 2010), (ii) a simplified reactive chlorine cycling mechanism (Sander et al., 2010), and (iii) the uptake of N_2O_5 on the chloride-containing particles (Bertram and Thornton, 2009).considered only simple chlorine reactions. Therefore, we attempted to incorporate the multi-phase halogen reactions into the CMAQ v5.2.1 model to investigate the influences of atmospheric halogen chemistrieschemistry. Detailed descriptions of these reactions are provided in the subsequent sections.

2.4.1 Chlorine reactions

The chlorine-related reactions were incorporated into the framework of SAPRC07-TC mechanism. The chlorine reactions consist of: (i) adjusted reaction rate coefficients for 14 reactions (refer to R9 to R22 in Table 1); (ii) updated 29 gaseous chlorine reactions (refer to R23 to R51 in Table 1); (iii) added two aqueous-phase reactions (refer to R1 to R2 in Table 2); and (iv) incorporated four heterogeneous reactions involving three reactive halogen species, HOCl, ClNO$_2$, and ClONO$_2$, with NO$_2$ partitioning onto chloride-containing particles (refer to R2 to R6 in Table 3).

The parameterization of γ_{N2O5} currently embedded in the CMAQ v5.2.1 model (shown in R8) has not been greatly satisfactory for reproducing the atmospheric levels of ClNO$_2$.

$$N_2O_5 + (1-\varphi)H_2O + \varphi Cl^{-1} \xrightarrow{\gamma_{N2O5}} (2-\varphi)HNO_3 + \varphi ClNO_2 \qquad (R8)$$
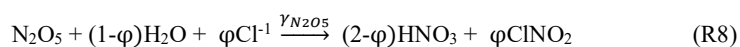
where, φ represents the yield of ClNO$_2$ as a function of the concentration of particulate chloride [Cl$^-$] and aerosol water content [H$_2$O]. The calculation of φ was proposed by Bertram and Thornton (2009):

$$\varphi = \frac{1}{1+\frac{[H2O]}{483[Cl-]}} \qquad (Eq. 3)$$

13

279   Although the use of R8 and Eq. 3 have been an advance in considering the production

280   of ClNO$_2$ from chlorine-containing particles (Bertram and Thornton, 2009), several studies

281   have reported that the parameterizations of γ_{N2O5} with R8 and Eq. 3 tend to produce excessive

282   amounts of nitrate and ClNO$_2$ (Riedel et al., 2012a; Li et al., 2016; Yu et al., 2020). This

283   overestimation may result from uncertainties in calculating aerosol water content ([H$_2$O])

284   estimated from the aerosol thermodynamic module (Chang et al., 2016). To deal with this issue,

285   several studies have explored different parameterizations of γ_{N2O5}. However, the γ_{N2O5} still

286   appears to be over-estimated in many cases (e.g., Chang et al., 2016; Liu et al., 2019; Mcduffie

287   et al., 2018; Riedel et al., 2012a; Wang et al., 2017). In this context, we alternatively selected

288   a different parameterization for γ_{N2O5} (see equations (4) to (7)). These parameterizations

289   were suggested by Riemer et al. (2003) and Evans and Jacob (2005):

290
$$\gamma_{N2O5} = f \times \gamma_1 + (1- f) \times \gamma_2 \qquad \text{(Eq. 4)}$$

291
$$f = \frac{m_{sulfate}}{m_{sulfate} + m_{nitrate}} \qquad \text{(Eq. 5)}$$

292
$$\gamma_1 = \alpha \times 10^\beta \qquad \text{(Eq. 6)}$$

293
$$\gamma_2 = 0.1 \times \gamma_1 \qquad \text{(Eq. 7)}$$

294   where α is set to be $2.79 \times 10^{-4} + 1.3 \times 10^{-4} \times RH - 3.43 \times 10^{-4} \times RH^2 + 7.52 \times 10^{-8} \times RH^3$.

295   β is set at 0.48, when T < 282 K, or at $4 \times 10^{-2} \times (294 - T)$, when T $\geq$ 282 K. m_i represents

296   the aerosol mass concentration of species i. Complete lists of chlorine reactions embedded into

297   the SAPRC07TC mechanism are shown in Tables 1, 2, and 3.

14

298 **Table 1.** List of homogeneous chlorine reactions used in this study.

No	Reaction	Reaction rate	Reference
R1	$Cl_2 \xrightarrow{hv} 2Cl$	#1.0/<Cl$_2$>	1
R2	$ClNO \xrightarrow{hv} Cl + NO$	#1.0/<ClNO>	1
R3	$Cl + NO_2 + M = ClONO$	1.3e-30^-2.0&1.0e-10^-1.0&-1.0&0.6&1.0	1
R4	$Cl + NO_2 + M = ClNO_2$	1.8e-31^-2.0&1.0e-10^-1.0&-1.0&0.6&1.0	1
R5	$ClONO \xrightarrow{hv} Cl + NO_2$	#1.0/<ClONO>	1
R6	$Cl + NO_3 = ClO + NO_2$	2.4×10^{-11}	1
R7	$ClO + NO_2 = ClONO_2$	1.80e-31^-3.4&1.5e-11^-1.90&0.6&1.0	1
R8	$HOCl \xrightarrow{hv} Cl + OH$	#1.0/<HOCl>	1
R9	$ClONO_2 = Cl + NO_3$	#1.0/<ClONO$_{2\_1}$>	2
R10	$ClONO_2 = ClO + NO_2$	#1.0/<ClONO$_{2\_2}$>	2
R11	$Cl + NO + M = 2ClNO$	$7.70 \times 10^{-32}(\frac{T}{300})^{-1.8}$	2
R12	$ClNO_2 \xrightarrow{hv} Cl + NO_2$	#1.0/<ClNO$_2$>	2
R13	$Cl + HO_2 = HCl$	$1.4 \times 10^{-11}e^{270/T}$	2
R14	$Cl + HO_2 = ClO + OH$	$3.6 \times 10^{-11}e^{-375/T}$	2
R15	$Cl + O_3 = ClO$	$2.3 \times 10^{-11}e^{200/T}$	2
R16	$ClO + NO = Cl + NO_2$	$6.4 \times 10^{-12}e^{290/T}$	2
R17	$ClONO_2 = ClO + NO_2$	2.0×10^{-21}	2
R18	$Cl + ClONO_2 = Cl_2 + NO_3$	$6.5 \times 10^{-12}e^{135/T}$	2
R19	$ClO + HO_2 = HOCl$	$2.6 \times 10^{-12}e^{290/T}$	2
R20	$ClO + ClO = Cl_2 + O_2$	$1.0 \times 10^{-11}e^{-1590/T}$	2
R21	$OH + HCl = Cl$	$1.8 \times 10^{-12}e^{-250/T}$	2
R22	$Cl + H_2 = HCl + HO_2$	$3.1 \times 10^{-11}e^{-2270/T}$	2
R23	$ClO + O = Cl + O_2$	$2.8 \times 10^{-11}e^{85/T}$	2
R24	$ClO + OH = Cl + HO_2$	$7.4 \times 10^{-12}e^{270/T}$	2
R25	$ClO + OH = HCl + O_2$	$6.0 \times 10^{-13}e^{230/T}$	2
R26	$HOCl + OH = ClO + H_2O$	$3.0 \times 10^{-12}e^{-500/T}$	2
R27	$HOCl + O = ClO + OH$	1.7×10^{-13}	2
R28	$ClNO_2 + OH = HOCl + NO_2$	$2.4 \times 10^{-12}e^{-1250/T}$	2
R29	$ClONO_2 + O = ClO + NO_3$	$3.6 \times 10^{-12}e^{-840/T}$	2
R30	$ClONO_2 + OH = HOCl + NO_3$	$1.2 \times 10^{-12}e^{-330/T}$	2
R31	$HCl + O = Cl + OH$	$1.0 \times 10^{-11}e^{-3300/T}$	2
R32	$Cl + ClNO = NO + Cl_2$	$5.8 \times 10^{-11}e^{100/T}$	2
R33	$Cl + HOCl = OH + Cl_2$	$3.4 \times 10^{-12}e^{-130/T}$	2
R34	$ClO \xrightarrow{hv} Cl + O$	#1.0/<ClO>	2
R35	$Cl + H_2O_2 = HCl + HO_2$	$1.1 \times 10^{-11}e^{-980/T}$	2
R36	$OH + Cl_2 = HOCl + Cl$	$2.6 \times 10^{-12}e^{-1100/T}$	2
R37	$Cl + HNO_3 = HCl + NO_2$	2.0×10^{-16}	2
R38	$Cl_2O_2 \xrightarrow{hv} Cl + ClO_2$	#1.0/<Cl$_2$O$_2$>	2
R39	$ClO_2 \xrightarrow{hv} ClO + O_2$	#1.0/<ClO$_2$>	2
R40	$Cl + ClO_2 = 2ClO$	1.2×10^{-11}	2
R41	$Cl + ClO_2 = Cl_2 + O_2$	2.3×10^{-10}	2
R42	$OH + Cl_2O_2 = HOCl + ClO_2$	$6.0 \times 10^{-13}e^{670/T}$	2
R43	$OH + ClO_2 = HOCl + O_2$	$1.4 \times 10^{-12}e^{600/T}$	2
R44	$Cl_2 + O_2 + M = Cl_2O_2$	2.2e-33^3.1&1.8e-10^0&-1.0&0.6&1.0	2
R45	$ClO + ClO + M = ClO_2$	1.9e-32^3.6&3.7e-12^1.6&-1.0&0.6&1.0	2
R46	$ClO_2 + O = ClO$	$2.4 \times 10^{-12}e^{-960/T}$	2
R47	$NO + ClO_2 = ClO + NO_2$	$6.0 \times 10^{-13}e^{-670/T}$	2
R48	$HCl + NO_3 = HNO_3 + Cl$	5.0×10^{-17}	2
R49	$Cl + Cl_2O_2 = Cl_2 + ClO$	$6.2 \times 10^{-11}e^{130/T}$	2
R50	$ClO + O_3 = ClO_2$	$2.0 \times 10^{-12}e^{-3600/T}$	2
R51	$ClO + NO_3 = ClO_2 + NO_2$	4.7×10^{-13}	2

299 1. Sander et al. (2010); 2. Burkholder et al. (2020)

Table 2. List of aqueous-phase chlorine and bromine reactions used in this study.

No	Species	Reaction	Reaction rate (unit: M/s)	Reference
R1	HOCl~~HOCl~~	$HOCl + HSO_3^- \xrightarrow{k} SO_4^{2-} + Cl^- + 2H^+$	2.8×10^5	1
R2	HOCl	$HOCl + SO_3^{2-} \xrightarrow{k} SO_4^{2-} + HCl$	7.6×10^8	1
R3	HOBr	$HOBr + HSO_3^- \xrightarrow{k} SO_4^{2-} + HBr$	5.0×10^9	1
R4	HOBr	$HOBr + SO_3^{2-} \xrightarrow{k} SO_4^{2-} + HBr$	2.6×10^7	1

1. Liu and Abbatt. (2020)

Table 3. List of heterogeneous halogen reactions and the uptake coefficients of gases used in this study.

No	Gas	Reaction	Uptake Coefficient (γ_{gas})	Reference
R1	N_2O_5	$N_2O_5 + (1-\varphi)H_2O + \varphi Cl^- \rightarrow (2-\varphi) HNO_3 + \varphi ClNO_2$	Function of aerosol mass concentrations, relative humidity, and temperature	1, 2
R2	HOCl	$HOCl + Cl^- = Cl_2$	1.09×10^{-3}	3
R3	$ClONO_2$	$ClONO_2 + Cl^- = Cl_2 + NO_3^-$	0.002	4
R4	$ClNO_2$	$ClNO_2 + Cl^- + H^+ = Cl_2 + HONO$	2.65×10^{-6} (pH < 2.0)	5
R5	$ClNO_2$	$ClNO_2 = Cl^- + NO_3^- + 2H^+$	6×10^{-6} (pH > 2.0)	6
R6	NO_2	$2NO_2 + Cl^- = ClNO + NO_3^-$	10^{-4}	7
R7	HOBr	$HOBr + Br^- = Br_2$	0.08	8
R8	HOBr	$HOBr + Cl^- = BrCl$	0.02	8
R9	$BrONO_2$	$BrONO_2 + H_2O = HOBr + HNO_3$	0.03	9
R10	HBr	$HBr = Br^-$	$1.3 \times 10^{-8}e^{\frac{4290}{T}}$	10
R11	$IONO_2$	$IONO_2 + Cl^- = ICl + HNO_3$	0.005	11
R12	$IONO_2$	$IONO_2 + Br^- = IBr + HNO_3$	0.005	11
R13	INO_2	$INO_2 + Cl^- = ICl + HONO$	0.01	11
R14	INO_2	$INO_2 + Br^- = IBr + HONO$	0.01	11
R15	HOI	$HOI + Cl^- = ICl$	0.005	12
R16	HOI	$HOI + Br^- = IBr$	0.005	12
R17	I_2O_2	$I_2O_2 =$	0.02	12
R18	I_2O_3	$I_2O_3 =$	0.02	12
R19	I_2O_4	$I_2O_4 =$	0.02	12

1. Riemer et al. (2003); 2. Evans and Jacob (2005); 3.Pratte and Rossi (2006); 4.Chen et al. (2022); 5.Riedel et al. (2012); 6.Roberts et al. (2009); 7.Abbatt and Waschewsky (1998); 8.Fernandez et al. (2014); 9.Deiber et al. (2004); 10.Ammann et al. (2013); 11.Saiz Lopez et al. (2014); 12.Sherwen et al. (2016)

2.4.2 Bromine reactions

We also incorporated bromine reactions into the SAPRC07-TC mechanisms. The reactions incorporated include: (i) updated absorption cross-sections for BrCl, BrCHO, $CHBr_2Cl$, $CHBr_3$, and $CHBrCl_2$ (refer to R29 to R33 in Table 4); (ii) updated reaction rates for formaldehyde (HCHO) and acetaldehyde (CH_3CHO~~CCHO~~) reacting with bromine radicals (refer to R34 and R35 in Table 4); (iii) Br-initiated VOC reactions (refer to R36 to R56 in Table 4); (iv) two inter-halogen species reactions (refer to R57 and R58 in Table 4); (v) two aqueous-phase reactions (refer to R3 to R4 in Table 2); and (vi) four heterogeneous reactions for bromine species (refer to R7 to R10 in Table 3). A complete list of the bromine reactions can be found in Tables 2, 3, and 4.

17

319   **Table 4**. List of homogeneous bromine reactions used in this study.

No	Reaction	Reaction rate	Reference
R1	$BrO \overset{hv}{\rightarrow} Br + O^3P$	#1.0/<BrO>	1
R2	$HOBr \overset{hv}{\rightarrow} Br + OH$	#1.0/<HOBr>	1
R3	$BrNO_3 \overset{hv}{\rightarrow} Br + NO_3$	#1.0/<BrNO$_3$_1>	1
R4	$BrNO_3 \overset{hv}{\rightarrow} BrO + NO_2$	#1.0/<BrNO$_3$_2>	1
R5	$BrNO_2 \overset{hv}{\rightarrow} Br + NO_2$	#1.0/<BrNO$_2$>	1
R6	$Br_2 \overset{hv}{\rightarrow} 2Br$	#1.0/<Br$_2$>	1
R7	$Br + O_3 = BrO$	$1.6 \times 10^{-11}e^{-780/T}$	1
R8	$BrO + HO_2 = HOBr$	$4.5 \times 10^{-12}e^{460/T}$	1
R9	$Br + HO_2 = HBr$	$4.8 \times 10^{-12}e^{-310/T}$	1
R10	$HBr + OH = Br$	$6.7 \times 10^{-12}e^{155/T}$	1
R11	$BrO + BrO = 2Br$	$1.4 \times 10^{-12}e^{210/T}$	1
R12	$BrO + BrO = Br_2$	$2.9 \times 10^{-14}e^{840/T}$	1
R13	$BrO + NO = Br + NO_2$	$8.8 \times 10^{-12}e^{260/T}$	1
R14	$Br + BrNO_3 = Br_2 + NO_3$	4.9×10^{-11}	1
R15	$Br_2 + OH = HOBr + Br$	$2.1 \times 10^{-11}e^{240/T}$	1
R16	$BrO + OH = Br + HO_2$	$1.7 \times 10^{-11}e^{250/T}$	1
R17	$Br + NO_3 = BrO + NO_2$	1.6×10^{-11}	1
R18	$BrO + ClO = Br + Cl$	$4.7 \times 10^{-12}e^{320/T}$	1
R19	$BrO + MEO2 = 0.8HOBR + 0.2BR + 0.3HCOOH + 0.2HCHO + 0.13OH + 0.13HO_2$	$2.65 \times 10^{-14}e^{1600/T}$	1
R20	$CH3Br + OH = Br$	$1.42 \times 10^{-12}e^{-1150/T}$	1
R21	$MB3^a + OH = 3Br$	$9.0 \times 10^{-13}e^{-360/T}$	1
R22	$MB2^b + OH = 2Br + HO_2$	$2.0 \times 10^{-12}e^{-840/T}$	1
R23	$MB2C^c + OH = 2Br + Cl$	$9.0 \times 10^{-13}e^{-420/T}$	1
R24	$MBC2^d + OH = Br + 2Cl$	$9.4 \times 10^{-13}e^{-510/T}$	1
R25	$MBC2^e + OH = Br + Cl + HO_2$	$2.1 \times 10^{-12}e^{-880/T}$	1
R26	$DMS + BrO = 0.75SO_2 + 0.25MSA + MEO2 + Br$	$1.5 \times 10^{-14}e^{1000/T}$	1
R27	$BrO + NO_2 = BrNO_3$	5.2e-31^3.2&6.9e-12^-2.9&0.6&1.0	1
R28	$Br + NO_2 = BrNO_2$	4.2e-31^2.4&2.7e-11^0.0&0.6&1.0	1
R29	$BrCl \overset{hv}{\rightarrow} Br + Cl$	#1.0/<BrCl>	2
R30	$FMBR^f \overset{hv}{\rightarrow} Br + CO + HO2$	#1.0/<FMBR>	2
R31	$MB3^a \overset{hv}{\rightarrow} 3.0Br + HO_2$	#1.0/<MB3>	2
R32	$MB2C^c \overset{hv}{\rightarrow} 2.0Br + Cl + HO_2$	#1.0/<MB2C>	2
R33	$MBC2^d \overset{hv}{\rightarrow} Br + 2.0Cl + HO_2$	#1.0/<MBC2>	2
R34	$HCHO + Br = HBr + HO_2$	$7.7 \times 10^{-12}e^{-580/T}$	2
R35	$CCHO + Br = HBr + MECO_3$	$1.8 \times 10^{-11}e^{-460/T}$	2
R36	$ETHE + Br = FMBR^f + HCHO + HO2 + RO2C$	1.3×10^{-13}	2
R37	$OLE1 + Br = FMBR^f + CCHO + HO2 + RO2C$	3.6×10^{-12}	2
R38	$OLE2 + Br = FMBR^f + 0.75RCHO + 0.15ACET + 0.1MEK + HO2 + RO2C$	1.0×10^{-11}	2
R39	$ISOPRENE + Br = FMBR^f + PRD2 + HO2 + RO2C$	7.5×10^{-11}	2
R40	$FMBR^f + OH = Br + CO$	5.0×10^{-12}	2
R41	$RCHO + Br = HBr + RCO3$	$1.8 \times 10^{-11}e^{-460/T}$	2
R42	$GLY + Br = HBr + 2CO + HO2$	$7.7 \times 10^{-12}e^{-580/T}$	2
R43	$MGLY + Br = HBr + CO + MECO3$	$1.8 \times 10^{-11}e^{-460/T}$	2
R44	$BALD + Br = HBr + BZCO3$	$1.8 \times 10^{-11}e^{-460/T}$	2
R45	$ACROLEIN + Br = 0.75\ FMBR^f + 0.25HBr + 0.25MACO3 + 0.75MGLY + 0.75HO2$	1.0×10^{-11}	2
R46	$Benzene + Br = Product$	1.0×10^{-11}	3
R47	$Toluene + Br = Product$	1.0×10^{-14}	4
R48	o-xylene + Br = Product	1.6×10^{-14}	4
R49	m-xylene + Br = Product	7.9×10^{-14}	4
R50	p-xylene + Br = Product	4.0×10^{-14}	4
R51	α-pinene + Br = Product	6.8×10^{-14}	5
R52	$MACR + Br = Product$	3.9×10^{-10}	5
R53	$MVK + Br = Product$	2.3×10^{-10}	5
R54	$MEK + Br = Product$	3.6×10^{-10}	5
R55	$ETOH + Br = Product$	$8.6 \times 10^{-11}e^{45/T}$	5
R56	$MEOH + Br = Product$	5.5×10^{-11}	5
R57	$Cl + BrCl = Br + Cl_2$	1.45×10^{-11}	6
R58	$Cl + Br_2 = BrCl + Br$	1.94×10^{-10}	7

320 1. Sherwen et al. (2016); 2. Burkholder et al. (2020); 3. Keefer et al. (1950); 4. Giri et al. (2022); 5. Qinyi et al. (2021); 6. Clyne and Cruse.
321 (1972); 7.Khamaganov and Crowley. (2010)
322 $MB3^a = CHBr_3$, $MB2^b = CH_2Br_2$, $MB2C^c = CH_2Br_2$, $MBC2^d = CHBr_2Cl$, $MBC^e = CH_2ClBr$, $FMBR^f = BrCHO$

2.4.3 Iodine reactions

Iodine reactions taken into account in this study were acquired from Saiz-Lopez et al. (2014) and Sherwen et al. (2016). We updated iodine reactions in three ways: (i) updated absorption cross-sections for ICl and IBr (refer to R43 and R44 in Table 5); (ii) two inter-halogen species reactions (refer to R45 and R46 in Table 5); and (iii) nine heterogeneous reactions for $IONO_2$, INO_2, HOI, I_2O_2, I_2O_3, and I_2O_4 (refer to R11 to R19 in Table 3). These iodine reactions are shown in Tables 3 and 5.

330 **Table 5.** List of homogeneous iodine reactions used in this study.

No	Reaction	Reaction rate	Reference
R1	$I_2 \overset{h\nu}{\to} 2I$	#1.0/<I_2>	1
R2	$HOI \overset{h\nu}{\to} I + OH$	#1.0/<HOI>	1
R3	$IO \overset{h\nu}{\to} I + O^3P$	#1.0/<IO>	1
R4	$OIO \overset{h\nu}{\to} I$	#1.0/<OIO>	1
R5	$INO \overset{h\nu}{\to} I + NO$	#1.0/<INO>	1
R6	$INO_2 \overset{h\nu}{\to} I + NO_2$	#1.0/<INO_2>	1
R7	$IONO_2 \overset{h\nu}{\to} I + NO_3$	#1.0/<$IONO_2$>	1
R8	$I_2O_2 \overset{h\nu}{\to} I + OIO$	#1.0/<$IONO_2$>	1
R9	$I_2O_3 \overset{h\nu}{\to} IO + OIO$	#1.0/<$IONO_2$>	1
R10	$I_2O_4 \overset{h\nu}{\to} 2OIO$	#1.0/<$IONO_2$>	1
R11	$CH_3I \overset{h\nu}{\to} I + MEO2$	#1.0/<CH_3I>	1
R12	$MIC \overset{h\nu}{\to} I + Cl$	#1.0/<MIC>	1
R13	$MIB \overset{h\nu}{\to} I + Br$	#1.0/<INO_2>	1
R14	$MI2 \overset{h\nu}{\to} 2I$	#1.0/<$IONO_2$>	1
R15	$I + O_3 = IO$	$2.1 \times 10^{-11}e^{-830/T}$	2
R16	$I + HO_2 = HI$	$1.5 \times 10^{-11}e^{-1090/T}$	2
R17	$I_2 + OH = HOI + I$	2.1×10^{-10}	2
R18	$HI + OH = I$	$1.6 \times 10^{-11}e^{440/T}$	2
R19	$HOI + OH = IO$	5.0×10^{-12}	2
R20	$IO + HO_2 = HOI$	$1.4 \times 10^{-11}e^{540/T}$	2
R21	$IO + NO = I + NO_2$	$7.15 \times 10^{-12}e^{300/T}$	2
R22	$INO + INO = I_2 + 2NO$	$8.4 \times 10^{-11}e^{-2620/T}$	2
R23	$INO_2 + INO_2 = I_2 + NO_2$	$4.7 \times 10^{-13}e^{-1670/T}$	2
R24	$I_2 + NO_3 = I + IONO_2$	1.5×10^{-12}	2
R25	$IONO_2 + I = I_2 + NO_3$	$9.1 \times 10^{-11}e^{-146/T}$	2
R26	$I + BrO = IO + Br$	1.2×10^{-11}	2
R27	$IO + Br = I + BrO$	2.7×10^{-11}	2
R28	$IO + BrO = Br + I$	$1.5 \times 10^{-11}e^{510/T}$	2
R29	$IO + ClO = I + Cl$	$4.7 \times 10^{-12}e^{280/T}$	2
R30	$OIO + OIO = I_2O_4$	1.5×10^{-10}	2
R31	$OIO + NO = IO + NO_2$	$1.1 \times 10^{-12}e^{542/T}$	2
R32	$IO + IO = 0.4OIO + 0.4I + 0.6I_2O_2$	$5.4 \times 10^{-11}e^{180/T}$	2
R33	$IO + OIO = I_2O_3$	1.5×10^{-10}	2
R34	$I_2O_2 = OIO + I$	$2.5 \times 10^{-14}e^{-9770/T}$	2
R35	$I_2O_4 = 2OIO$	3.8×10^{-2}	2
R36	$INO_2 = NO_2 + I$	$9.9 \times 10^{17}e^{-11859/T}$	2
R37	$IONO_2 = NO_2 + IO$	$2.1 \times 10^{15}e^{-13670/T}$	2
R38	$CH_3I + OH = HCHO$	$4.3 \times 10^{-12}e^{-1120/T}$	2
R39	$IO + DMS = 0.75SO_2 + 0.25MSA + MEO2$	$3.3 \times 10^{-13}e^{-925/T}$	2
R40	$I + NO = INO$	1.8e-32^-1.0&1.7e-11^0.0&0.6&1.0	2
R41	$I + NO_2 = INO_2$	3.0e-31^-1.0&6.6e-11^0.0&0.6&1.0	2
R42	$IO + NO_2 = IONO_2$	7.7e-31^-3.5&7.7e-12^-.1.5&0.6&1.0	2
R43	$ICl \overset{h\nu}{\to} I + Cl$	#1.0/<ICl>	3
R44	$IBr \overset{h\nu}{\to} I + Br$	#1.0/<IBr>	3
R45	$Cl + I_2 = ICl + I$	2.81×10^{-10}	4
R46	$Br + I_2 = IBr + I$	1.2×10^{-10}	5

331 1. Sherwen et al. (2016); 2. Saiz-Lopez et al. (2014); 3. Burkholder et al. (2020); 4. Baklanov et al. (1997);
332 5.Bedjanian et al. (1997)

333

2.5 Experimental design

To better understand the impacts of atmospheric halogen ~~chemistries~~chemistry, we designed four experiments: (i) experiment without halogen chemistry (referred to as CTRL); (ii) original CMAQv5.2.1 model simulation only with chlorine processes (EXP_{Cl}); (iii) experiment with both chlorine and bromine processes (EXP_{Cl_Br}); and (iv) experiment with full halogen processes ($EXP_{Cl\_Br\_I}$). The design of these four experiments is explained in Table 6.

In addition, in order to further analyze our results, we carried out two more experiments: (i) CMAQ model runs with the halogen chemistry constructed by Saiz-Lopez et al. (2014) (labeled as EXP_{CAM}); and (ii) CMAQ model run with the halogen chemistry constructed by Sarwar et al. (2015) (labelled as EXP_{CMAQ}). The former halogen chemistry was included in a global CTM named CAM-Chem, while the latter was in the CMAQ model. That is why we labeled these two experiments, EXP_{CAM} and EXP_{CMAQ}, respectively.

Table 6. Description of the four experiments conducted in this study.

Experiment	Chlorine		Bromine		Iodine	
	Emission	Reaction	Emission	Reaction	Emission	Reaction
CTRL	-	-	-	-	-	-
EXP_{Cl}	√	√	-	-	-	-
EXP_{Cl_Br}	√	√	√	√	-	-
$EXP_{Cl\_Br\_I}$	√	√	√	√	√	√

3. Results & Discussions

In this section, we discuss the accuracy of new halogen ~~chemistries~~ chemistry and processes through the comparison between simulated and measured mixing ratios of halogen-containing compounds during the period of KORUS-AQ campaign. We then analyze the

353 experimental results to evaluate the impacts of atmospheric halogen ~~chemistries~~ chemistry and

354 processes on key-species concentrations in the atmosphere.

3.1 Model performances

3.1.1 Observed vs Modeled ClNO$_2$ mixing ratios

357   To evaluate the model performances, we used the mixing ratios of ClNO$_2$ observed at

358 two supersites (Olympic Park and Mt. Taehwa stations) in South Korea. Although the mixing

359 ratios of atmospheric Cl$_2$ were also measured at these two stations, we focused solely on ClNO$_2$

360 observations due to several uncertainties associated with Cl$_2$ analysis. These issues will be

361 discussed later in Sect. 3.1.3.

362   Figure 2 presents the diurnal variations of modeled and observed mixing ratios of

363 ClNO$_2$ at two monitoring stations. The CTRL simulation (black circles and lines in Fig. 2) and

364 EXP$_{CAM}$ (purple circles and lines in Fig. 2) could not reproduce the observed mixing ratios of

365 ClNO$_2$ at the two supersites. For instance, the average mixing ratios of ClNO$_2$ at both

366 monitoring stations were 0.00 ppt for CTRL and 15.40 ppt for EXP$_{CAM}$, while the observed

367 average mixing ratio of ClNO$_2$ was 122.67 ppt. This large discrepancy may be primarily due

368 to the absence of heterogeneous ClNO$_2$ formation via N$_2$O$_5$ in the halogen scheme

369 implemented for EXP$_{CAM}$, which was based on Saiz-Lopez et al. (2014). It is noted that this

370 mechanism was originally designed for clean, oceanic environments and does not account for

371 anthropogenic chlorine sources or inland ClNO$_2$ formation pathways, such as the reactions of

372 N$_2$O$_5$ with particulate chloride (recall R8: N$_2$O$_5$ + (1-φ)H$_2$O + ηCl$^-$ → (2-φ)HNO$_3$ +

373 φClNO$_2$). ~~The reason for these large differences may be attributed to uncertainties in the~~

374 ~~consideration of heterogeneous partitioning of N$_2$O$_5$ onto chloride-containing particles in the~~

375 ~~model (recall R8: N$_2$O$_5$ + (1-φ)H$_2$O + ηCl$^-$ → (2-φ)HNO$_3$ + φClNO$_2$).~~

376   On the other hand, the EXP$_{CMAQ}$ (blue circles and lines in Fig. 2) and EXP$_{Cl\_Br\_I}$ (red

377 circles and lines in Fig. 2), which accounted for halogen ~~chemistries~~chemistry, tend to better

capture the diurnal patterns of observed mixing ratios of $ClNO_2$ (refer to open circles and lines

in Fig. 2). These models also demonstrated significant improvements, in terms of statistical

metrics (which will be presented in Table 7).

Although the EXP_{CMAQ} showed reasonable agreement, it also exhibited significant

biases during the nighttime. Conversely, the $EXP_{Cl\_Br\_I}$ simulation achieved better agreements

with the observed mixing ratios of $ClNO_2$ at both stations. For example, the index of agreement

(IOA) increased from 0.62 for EXP_{CMAQ} to 0.66 for $EXP_{Cl\_Br\_I}$ and from 0.57 to 0.59 at

Olympic Park and Mt. Taehwa stations, respectively. These enhancements suggest that

successful implementation of the models depends on not only considering chlorine reactions

but also incorporating more comprehensive halogen reactions, as demonstrated by $EXP_{Cl\_Br\_I}$.

The following sections will explore and discuss these halogen reactions in the atmosphere.
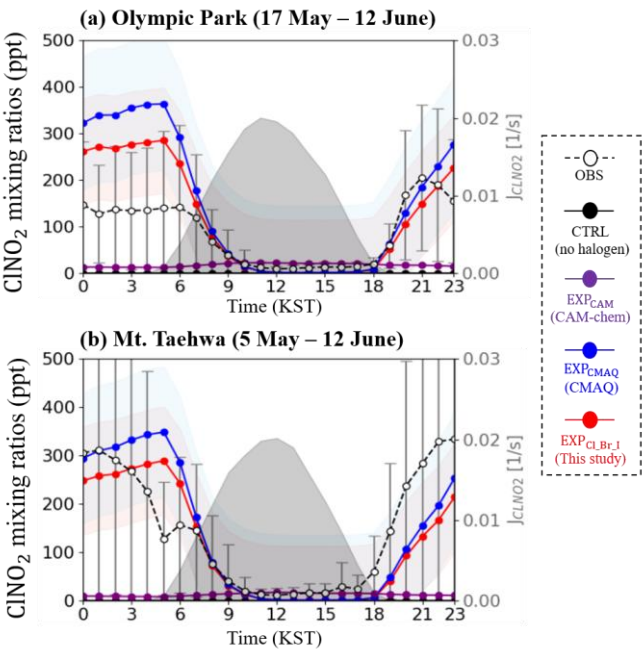

Figure 2. Diurnal variations in the mixing ratios of $ClNO_2$ (unit: ppt) at (a) Olympic Park and
(b) Mt.Taehwa stations during the period of the KORUS-AQ campaign. Observed values are

392 represented by open circles (error bars indicate the standard deviation). Colored lines with
393 shaded areas show the hourly-averaged mixing ratios of $ClNO_2$ and the corresponding standard
394 deviation from each simulation. The black shaded area indicates the variations in the photolysis
395 rate of $ClNO_2$ derived from the $EXP_{Cl\_Br\_I}$ simulation.

396 **Table 7.** Statistical metrics for $ClNO_2$ analysis from CTRL, EXP_{CAM}, EXP_{CMAQ}, and $EXP_{Cl\_Br\_I}$
397 simulations at the Olympic Park and Mt.Taewha stations during the period of KORUS-AQ
398 campaign.

Target: $ClNO_2$		Olympic Park	Mt.Taehwa
	Observed mean (ppt)	85.97	159.36
CTRL	Modeled mean (ppt)	0	0
	MB (ppt)	-85.97	-159.36
	RMSE (ppt)	150.30	288.82
	IOA	0.41	0.40
EXP_{CAM}	Modeled mean (ppt)	17.31	13.49
	MB (ppt)	-68.67	-145.87
	RMSE (ppt)	143.23	281.78
	IOA	0.37	0.40
EXP_{CMAQ}	Modeled mean (ppt)	135.77	152.89
	MB (ppt)	49.80	-6.65
	RMSE (ppt)	204.42	289.19
	IOA	0.62	0.57
$EXP_{Cl\_Br\_I}$	Modeled mean (ppt)	116.76	134.29
	MB (ppt)	30.79	-25.07
	RMSE (ppt)	174.41	272.69
	IOA	0.66	0.59

399

400 **3.1.2 Contributions to mixing ratios of ClNO₂**

401   Figure 3a and 3c represent the diurnal variations in the mixing ratios of $ClNO_2$ from

402 the EXP_{CMAQ} (blue dotted line) and $EXP_{Cl\_Br\_I}$ simulations (red dotted line) at two supersites

403 during the period of the KORUS-AQ campaign. Through a sensitivity test, we attempted to

404 identify the key reactions in the $EXP_{Cl\_Br\_I}$ causing differences from the EXP_{CMAQ} simulation.

405 From the studies, we identified four critical halogen reactions: (i) updated reaction rate

406 coefficient of R20 in Table 1; (ii) newly- added heterogeneous reaction of HOBr as shown in

407 R8 of Table 3; (iii) modified parameterization of γ_{N2O5} as shown in R1 of Table 3; and (iv)

408 newly- added heterogeneous reaction of NO_2 onto atmospheric aerosols as shown in R6 of

409 Table 3. The contributions of these four reactions were calculated and are presented in blue-,

410 green-, yellow-, and red-shaded areas in Fig. 3, respectively. It appears is evident that the

411 contribution of the parameterization of γ_{N2O5} is the most significant. A detailed analysis of

412 these differences between EXP_{CMAQ} and the $EXP_{Cl\_Br\_I}$ is further discussed in Table S2.

25

413   Figure 3b and 3d illustrate the contributions of the four reactions to the mixing ratios

414 of $ClNO_2$ at the two supersites. Our results again indicates that selecting the new γ_{N2O5} led

415 to the largest decreases in the averaged mixing ratios of $ClNO_2$ by 9.58 ppt (50.4%) and 7.50

416 ppt (40.3%) at the Olympic Park and Mt. Taehwa stations, respectively. These reductions are

417 obviously attributed to lower values of γ_{N2O5} in $EXP_{Cl\_Br\_I}$ (γ_{N2O5} = ~0.013), compared to

418 those in EXP_{CMAQ} (γ_{N2O5} = ~0.014) as shown in Fig. S3. Such a small difference in γ_{N2O5}

419 led to substantial differences in the mixing ratios of $ClNO_2$. In addition, the inclusion of

420 reaction (recall R20: $ClO + ClO \rightarrow Cl_2$), with its rate constant reduced by a factor of 10 from

421 the original CMAQ model (see Table S2), led to a 3.40 ppt (17.8%) decrease in the $ClNO_2$

422 mixing ratio at the Olympic Park station. This effect is likely due to the slower removal of ClO,

423 which resulted in slightly elevated ClO levels in the boundary layer. The increased ClO may

424 have promoted the formation of $ClONO_2$ (i.e., reservoir species) via reaction with NO_2, thereby

425 reducing the amount of reactive nitrogen available for $ClNO_2$ production through the

426 heterogeneous pathway. (R20) with a reaction rate coefficient reduced by a factor of 10,

427 contributed to the reduction in the mixing ratios of $ClNO_2$ by 3.40 ppt (17.9%) at the Olympic

428 Park station. Accounting for the heterogeneous reaction of NO_2 and HOBr onto chlorine-

429 containing particles also resulted in reductions in the mixing ratios of $ClNO_2$ by 4.46 ppt

430 (24.0%) and 2.77 ppt (14.9%) at the Mt. Taehwa station, respectively. These reactions

431 competitively consume chloride-containing particles, thereby reducing the availability of

432 particulate chlorine that is essential for $ClNO_2$ formation. Overall, these results indicate that

433 the reduction in the $ClNO_2$ mixing ratios was primarily driven by the updated chlorine

434 chemistry, particularly the revised parameterization of γ_{N2O5} and the inclusion of additional

435 chlorine-related reactions, with secondary contributions from bromine chemistry.

436   Collectively, the four reactions mentioned above may be the key reactions that can

437 significantly change the atmospheric levels of $ClNO_2$. Nevertheless, it should also be noted

438   that the $EXP_{Cl\_Br\_I}$ simulation still exhibited discrepancies with the observed mixing ratios of

439      $ClNO_2$. These remaining biases may be attributed to factors not fully accounted for in the

440   current modeling framework, including (i) the uptake of Cl_2 or related species onto aerosol

441   surfaces, (ii) uncertainties in the $ClNO_2$ yield, (iii) simplified diurnal emissions profiles for

442   HCl and Cl_2, and (iv) missing constrained halogen reactions. These limitations require further

443   targeted sensitivity analyses to better quantify their individual and combined impacts.

444   ~~. Further studies should investigate the factors causing these discrepancies (such as~~

445   ~~yield of $ClNO_2$ (φ_{ClNO2}), unknown chlorine emissions, and missing halogen reactions) to~~

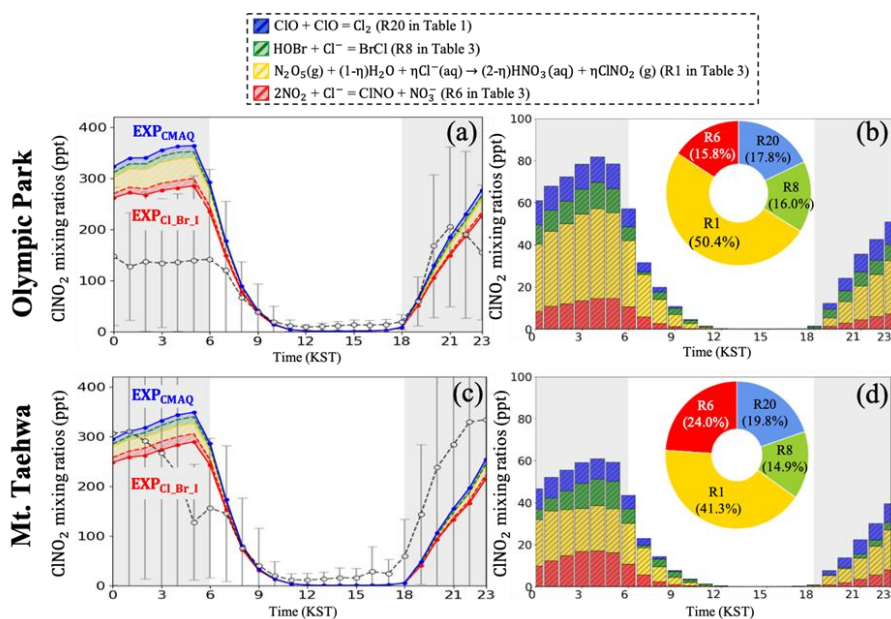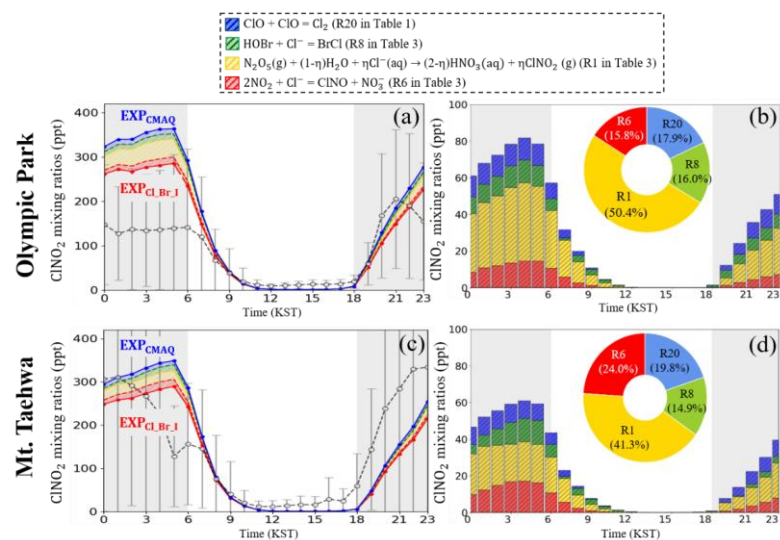446   ~~enhance our understanding of atmospheric halogen chemistry.~~

Figure 3. Contributions of halogen reactions to the mixing ratios of $ClNO_2$ in the EXP_{CMAQ} and $EXP_{Cl\_Br\_I}$ simulations at (a and b) Olympic Park and (c and d) Mt. Taehwa stations during the period of KORUS-AQ campaign. Stacked bars and pie charts show the contributions from four halogen reactions to the mixing ratios of $ClNO_2$. Grey-shaded areas represent nighttime (18:00-06:00 local standard time).

28

454
455
456

3.1.3 Uncertainties in Cl_2

457

Figure 4 represents bar graphs of <u>24-hour</u> average<u>d</u> Cl_2 mixing ratios from the four

458

experiments, together with the observed Cl_2 mixing ratios at two supersites. Among them, the

459

mixing ratios of Cl_2 from the $EXP_{Cl\_Br\_I}$ agree well with the observed mixing ratios of Cl_2.

460

Based on these findings, we attempted to analyze which reactions contributed to elevated levels

461

of Cl_2. Two key reactions were identified: (i) $HOCl + Cl^- \rightarrow Cl_2$ (R2 in Table 3) and (ii)

462

$ClONO_2 + Cl^- \rightarrow Cl_2$ (R3 in Table 3). These reactions accounted for<u> an increase in</u> Cl_2

463

~~increase~~ of 0.18 ppt (14.2%) and 1.06 ppt (84.1%), respectively, at the two supersites.

464

Although the current modeling system has improved the predictions of 'campaign-

465

averaged' Cl_2 mixing ratios, it has a serious limitation in reproducing daytime Cl_2 levels, likely

466

due to the extremely fast photo-dissociation rate of Cl_2 (J_{Cl2} is estimated at 2.5×10^{-3} s^{-1}). In

467

other words, once Cl_2 was produced via daytime halogen reaction pathways (see R3 to R5 in

468

Table 3), it ~~is~~ <u>was</u> rapidly removed by the fast photo-dissociation. To address this challenge,

469

several studies suggested potential missing daytime reactions, such as particulate nitrate

470

photolysis and the uptake of O_3 and OH onto atmospheric particles (Peng et al., 2022; Chen et

471

al., 2022). However, these reactions also have limitations in perfectly explaining the relatively

472

high levels of Cl_2 during the daytime. <u>Although the model slightly overestimates Cl_2 mixing</u>

473

<u>ratios during the nighttime (by approximately 0.3 ppt), the major discrepancy lies in the</u>

474

<u>inability to capture daytime peaks. In this context, the</u>~~The~~ accuracy of simulating daytime Cl_2

475

mixing ratios remains a topic of further discussion.

476

In addition, significant uncertainties have been reported in observing Cl_2 mixing ratios

477

using the CIMS instrument. The detection limit for Cl_2 in the CIMS instrument was estimated

478

to be 2.9 ppt over a 30-minute interval (Jeong et al., 2019). However, the averaged mixing

479

480 ratios of Cl_2 of 2.08 ppt and 2.69 ppt were measured at Olympic Park and Mt. Taehwa,

481 respectively, as depicted in Fig.4. Given that the observed levels of Cl_2 at the two monitoring

482 stations were very close to the detection limit of the instrument, significant uncertainties likely

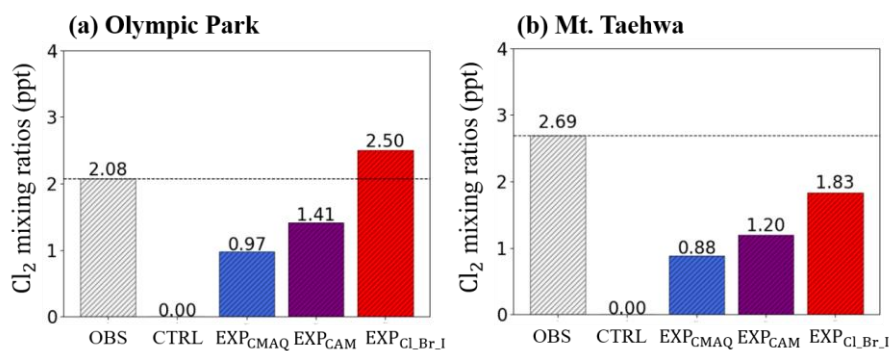483 exist in these measurements of the mixing ratios of Cl_2.

484

485

Figure 4. Comparisons of averaged mixing ratios of Cl_2 observed (OBS) and modeled from four simulations (CTRL, EXP_{CMAQ}, EXP_{CAM}, and $EXP_{Cl\_Br\_I}$) at (a) Olympic Park and (b) Mt. Taehwa stations. Dotted lines represent the observed mixing ratios of Cl_2.

3.1.4 Levels of bromine monoxide (BrO) and iodine monoxide (IO)

To strengthen the model evaluation, we also compared simulated bromine monoxide (BrO) and iodine monoxide (IO) levels with previously reported observational and modeling data, as shown in Fig. 5.

As illustrated in Fig. 5a, several modeling studies reported the mixing ratios of BrO ranging from 0.0 to 1.3 ppt (Koenig et al., 2017; Le Breton et al., 2017; Fan and Li, 2022; Zhu et al., 2019; Li et al., 2020; Li et al., 2019), which are similar to observed values (Koenig et al., 2017; Peters et al., 2005). Our simulation results indicate relatively low BrO mixing ratios, which may be attributed to low levels of chlorophyll-a over the Korean Peninsula during May and June (Son, 2013).

500   For IO, previous field and modeling studies have reported the mixing ratios of IO

501   ranging from 0.0 to 2.5 ppt (Großmann et al., 2013; Allan et al., 2000; Fan and Li, 2022; Li et

502   al., 2020; Takashima et al., 2021; Prados-Román et al., 2015; Mahajan et al., 2012; Mahajan et

503   al., 2010; Inamdar et al., 2020). Overall, our simulated IO mixing ratios (0.0 – 1.8 ppt) over

504   the East Asian ocean region during the KORUS-AQ campaign is comparable to previously

505   reported ranges, as shown in Fig. 5b.

506   Although BrO and IO were not directly measured during the KORUS-AQ campaign,

507   this comparison suggests that our simulated halogen species are within a reasonable range of

508   previously reported values. These indirect evaluations complement the ClNO$_2$-based validation

509   and enhance confidence in our model's ability to simulate regional-scale behavior of bromine
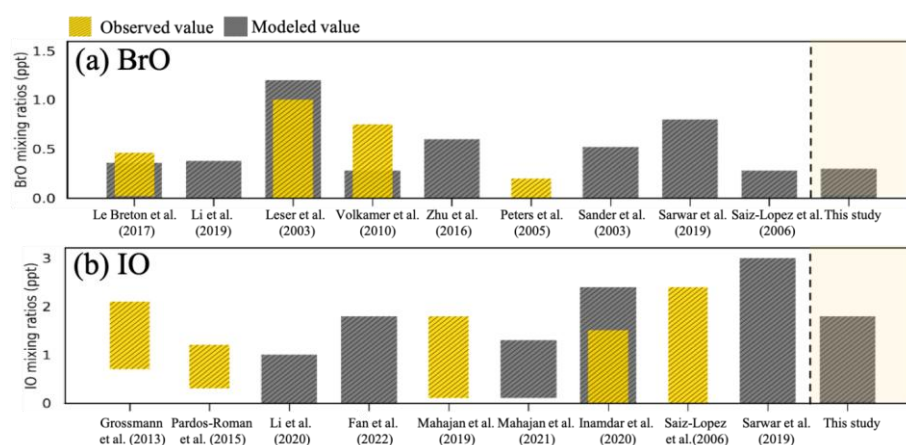
510   and iodine species.

Figure 5. Comparisons between modeled and observed mixing ratios of atmospheric (a) BrO and (b) IO. Both are observed and modeled mixing ratios were obtained from the previous studies.

3.2 Influences of halogen chemistry on O_3 mixing ratios

3.2.1 Comparative analysis at three supersites

Based on the evaluation of model performances, we analyzed the impacts of halogen processes on atmospheric O_3 mixing ratios at three monitoring stations (regarding the locations, see Fig. 1a). Fig. ~~5~~ 6 represents the diurnal variations in the mixing ratios of O_3 as simulated from both the CTRL (black circles) and $EXP_{Cl\_Br\_I}$ (red circles), together with the observations (white open circles) during the period of the KORUS-AQ campaign. It shows that the O_3 mixing ratios simulated from the $EXP_{Cl\_Br\_I}$ slightly increased by ~0.06 ppb (0.3%) and ~0.14 ppb (0.4%), higher than those from the CTRL at Olympic Park and Mt. Taehwa stations, respectively. Similar patterns were also observed in the comparisons between O_3 observations from 320 AIR-KOREA stations and O_3 predictions (as shown in Fig. S4).

It should be noted that the simulated O_3 mixing ratios decreased slightly by ~0.19 ppb (0.3%), lower than those simulated from the CTRL at the Bangnyung station. These results raised two questions: (i) why did the opposite patterns take place between two land stations and one ocean station (Bangnyung Island station)? and (ii) what mechanism caused these opposite patterns in the mixing ratios of O_3? To answer these two questions, we further investigated the role of halogen chemistry in atmospheric O_3 chemistry.
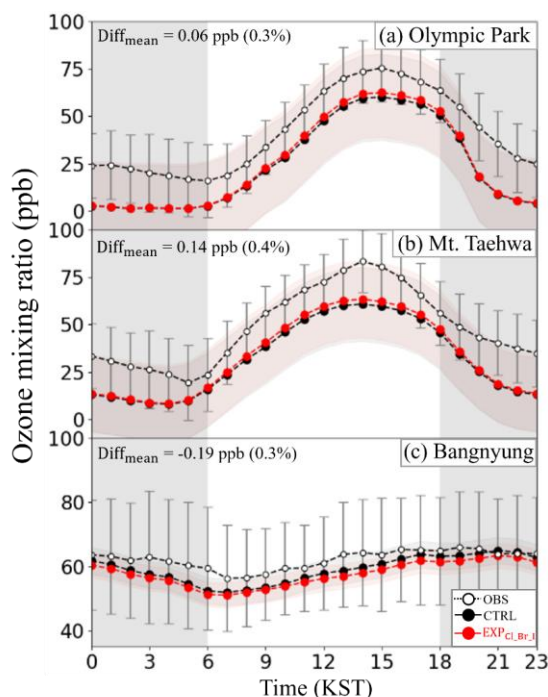
32

533

33
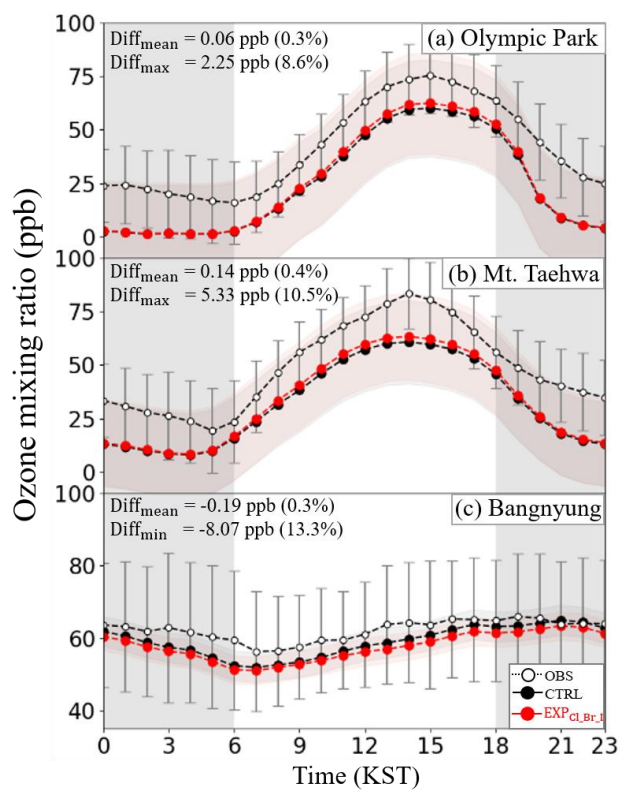
Figure 5̶6. Diurnal variations in the mixing ratios of O_3 from CTRL (black circles) and $EXP_{CL\_Br\_I}$ (red circles) simulations, together with observed mixing ratios of O_3 (OBS; white circles) at (a) Olympic Park, (b) Mt. Taehwa, and (c) Bangnyung stations during the period of the KORUS-AQ campaign. Error bars and grey-shaed areas represent one standard deviations and nighttime, respectively. Error bars and shaded areas indicate the standard deviations of observed and modeled O_3, while the grey-shaded areas show the nighttime. $DIFF_{mean}$ represents the difference in the averaged mixing ratios of O_3 between $EXP_{Cl\_Br\_I}$ and CTRL simulations.

3.2.2 Impacts of halogen processes

Figure 6̶ 7 illustrates the spatial distributions of the differences between two O_3 mixing

ratios simulated under the consideration of individual halogen chemistries chemistry over the

Korean peninsula. The CMAQ-simulated O_3 mixing ratios for EXP_{Cl} showed an increase of

0.62 ppb (1.4%) compared to those from the CTRL over the Korean peninsula (as shown in

Fig. 7̶6a). This increase is attributed to the VOC oxidation by Cl radicals, which leads to the

34

production of additional RO_2 radicals. Additional O_3 is subsequently produced via the RO_2 + NO reactions. It is well-known that VOC oxidation rates by Cl radicals are approximately 10 times faster than those by OH radicals (Edwards and Young, 2024). Several previous studies have also confirmed these findings (Kim et al., 2023; Jo et al., 2023).

Bromine-containing species are known to contribute to O_3 destruction in the atmosphere. However, VOC oxidations by Br radicals also contribute to atmospheric O_3 formation via the reactions of Br + VOC → products + RO_2 (these reactions are shown in R36 to R57 in Table 4). As a result, the net effects of bromine processes (i.e., $EXP_{Cl\_Br} - EXP_{Cl}$) lead to a slight increase in O_3 mixing ratios of ~0.01 ppb, as shown in Fig. 7b. This negligible increase is likely due to the competition between O_3 loss via bromine-catalyzed destruction and O_3 production via VOC oxidation. slightly increase O_3 mixing ratios by ~0.01 ppb, as shown in Fig. 6b. These negligible effects are likely because the decrease in O_3 mixing ratios is almost offset by an increase in O_3 mixing ratios.

In Fig. 7c, when iodine processes were incorporated into the modeling system, the surface-averaged O_3 mixing ratios decreased by ~1.39 ppb (2.4%), particularly over ocean areas. The iodine radicals generated from the photolysis of marine-originated iodine species primarily react with O_3. Given the low levels of VOCs over ocean areas, iodine radicals predominantly participate in the O_3 destruction over the ocean.

Again, the O_3 mixing ratios are controlled by competition between the O_3 production and O_3 destruction. We found that the average O_3 mixing ratios increased by 0.21 ppb (~0.5%) over land areas and decreased by 0.69 ppb (~1.2%) over ocean areas under the considerations of entire halogen processes (i.e., $EXP_{Cl\_Br\_I} - CTRL$) (refer to Figs. 7d and S5). These findings are closely in line with the increases in O_3 mixing ratios at the Olympic Park and Mt. Taehwa stations (located on land areas) and the decreases in O_3 mixing ratios at the Bangnyung station (located around ocean areas) under the comprehensive considerations of the halogen

575 ~~chemistries~~chemistry, as discussed in Sect. 3.2.1. Such contrasting effects of halogen chemistry

576 between polluted continental and pristine oceanic regions are consistent with previous studies

577 (e.g., Li et al., 2022; Saiz-Lopez et al., 2023), which have also reported O_3 enhancements over

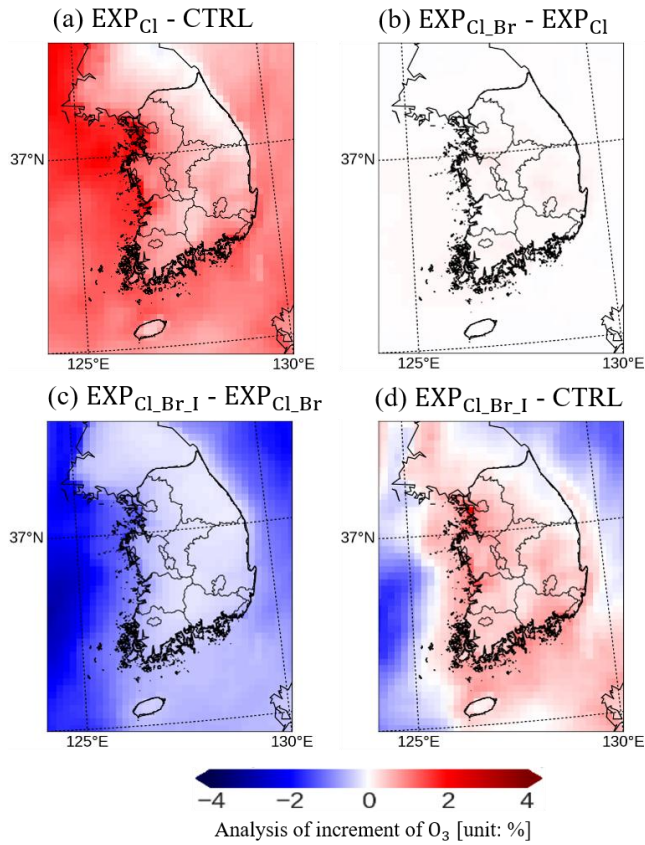578 land and reductions over the ocean.

579

(a) EXP$_{Cl}$ - CTRL   (b) EXP$_{Cl\_Br}$ - EXP$_{Cl}$

(c) EXP$_{Cl\_Br\_I}$ - EXP$_{Cl\_Br}$ (d) EXP$_{Cl\_Br\_I}$ - CTRL

Analysis of increment of O$_3$ [unit: %]

Figure 76. Spatial impacts of (a) chlorine processes (EXP$_{Cl}$ - CTRL), (b) bromine processes (EXP$_{Cl\_Br}$ – EXP$_{Cl}$), (c) iodine processes (EXP$_{Cl\_Br\_I}$ – EXP$_{Cl\_Br}$), and (d) total halogen processes (EXP$_{Cl\_Br\_I}$ – CTRL) on O$_3$ mixing ratios over the Korean peninsula.

3.2.3 Net O$_x$ production

To better understand the influences of the halogen ~~chemistries~~ chemistry on atmospheric O$_3$ mixing ratios, we additionally carried out a quantitative analysis. We calculated O$_x$ production rates (P(O$_x$)) utilizing a definition of expanded O$_x$ family ($\equiv$ O$_3$ + O^{1D} + O^{3p} + NO$_2$ + 2NO$_3$ + 3N$_2$O$_5$ + XNO$_2$ + XO + XONO$_2$; here, X denotes Cl, Br, and I). The constructions of the P(O$_x$) are shown in equations (8) to (10):

37

$$F(O_x) = k_{HO_2+NO}[HO_2][NO] + k_{RO_2+NO}[RO_2][NO] \tag{Eq. 8}$$

$$D(O_x) = k_{NO_2+OH}[NO_2][OH] + k_{O_3+VOC}[O_3][VOC] + k_{O(1D)+H_2O}[O(^1D)][H_2O]$$

$$+ k_{O_3+OH}[O_3][OH] + k_{O_3+HO_2}[O_3][HO_2] + k_{RO_2+NO_2}[RO_2][NO_2]$$

$$+ (k_{XO+O_3}[O_3] + k_{XO+HO_2}[HO_2] + k_{XO+O(3p)}[O(^3P)])[XO]$$

$$+ k_{ClO+NO_2}[NO_2][ClO] + k_{XO+XO}[XO]^2 + k_{NO_3+VOC}[NO_3][VOC]$$

$$+ 3k_{het}[N_2O_5] \tag{Eq. 9}$$

$$+ k_{O_3+OH}[O_3][OH] + k_{O_3+HO_2}[O_3][HO_2] + k_{RO_2+NO_2}[RO_2][NO_2]$$

$$+ (k_{ClO+O_3}[O_3] + k_{ClO+NO_2}[NO_2] + k_{ClO+O(3p)}[O(^3P)])[ClO]$$

$$+ k_{Cl+O_3}[Cl][O_3] + k_{BrO+OH}[BrO][OH] + k_{XO+HO_2}[XO][HO_2]$$

$$+ k_{XO+XO}[XO]^2 + k_{NO_3+VOC}[NO_3][VOC] + 3k_{het}[N_2O_5] \tag{Eq. 9}$$

$$P(O_x) = F(O_x) - D(O_x) \tag{Eq. 10}$$

where, $F(O_x)$ and $D(O_x)$ represent the O_x formation rates and O_x destruction rates, respectively. k_i and k_{het} denote the reaction rate constants for reaction i and heterogeneous reactions of N_2O_5, respectively.

Figure 87 shows the average O_x formation rates ($F(O_x)$), O_x destruction rates ($D(O_x)$), and the $P(O_x)$ from the CTRL and $EXP_{Cl\_Br\_I}$ simulations. Over land, rates for reactions of RO_2 + NO and HO_2 + NO in the $F(O_x)$ increased from 2.16 ppb/h to 2.21 ppb/h and from 2.05 ppb/h to 2.09 ppb/h, respectively, with the full consideration of the halogen processes in the CMAQ model. On the contrary, $D(O_x)$ decreased from 1.12 ppb/h to 0.97 ppb/h due to the limited contribution of O_3 destruction by halogen radicals. Consequently, $P(O_x)$ increased from 3.08 ppb/h to 3.33 ppb/h. The enhanced $F(O_x)$ of 0.09 ppb/h with decreased $D(O_x)$ of 0.15 ppb/h contributes to the increase in $P(O_x)$ of 0.25 ppb/h. Consistent results were observed at the Olympic Park and Mt. Taehwa stations (as shown in Figs. 65a and 65b).

614　　　　On the other hand, the $F(O_x)$ decreased by 0.03 ppb/h, while both $D(O_x)$ and $P(O_x)$

615　　increased by 0.12 ppb/h and 0.14 ppb/h, respectively, over the ocean (refer to Fig. 8~~7~~b and

616　　Table 8). This may be caused by the halogen-related losses in $D(O_x)$ (caused mainly by IO+

617　　HO_2 reaction), significantly contributing to the O_3 destruction. ~~This indicates~~<u>These results</u>

618　　<u>indicate</u> that the mixing ratios of O_3 tend to decrease in the presence of iodine radicals over the

619　　ocean areas. This is also in line with the case of the Bangnyung station, shown in Fig. 6~~5~~c.
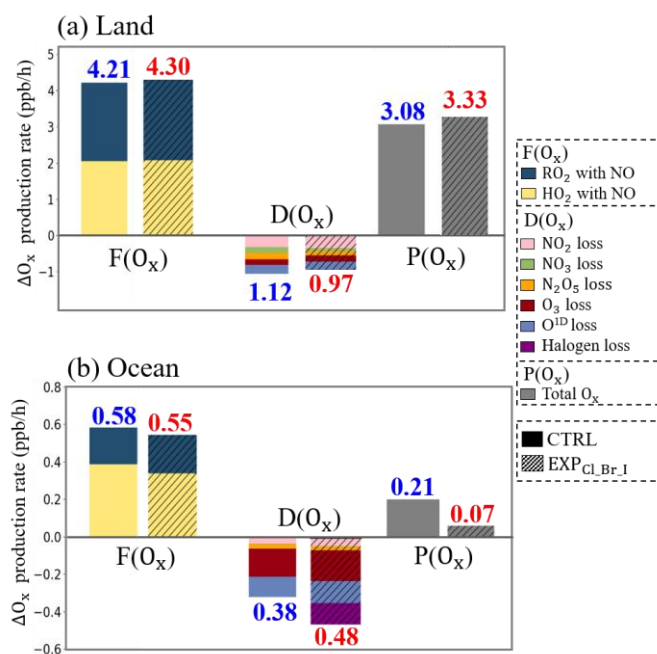

620

Figure 8~~7~~. The stacked bar graphs represent O_x formation rate ($F(O_x)$), destruction rate ($D(O_x)$), and production rate ($P(O_x)$) in the CTRL (plain bars) and $EXP_{Cl\_Br\_I}$ (hatched bars) simulations over the (a) land and (b) ocean areas, respectively, during the period of KORUS-AQ campaign. Individual reactions contributing to $F(O_x)$ and $D(O_x)$ are indicated by the bar colors.

Table 8. Averaged budget for O_x formation rates ($F(O_x)$), O_x destruction rates ($D(O_x)$), and O_x production rates ($P(O_x)$) calculated from the CTRL and $EXP_{Cl\_Br\_I}$ simulations during the period of KORUS-AQ campaign.

	Land		Ocean	
	CTRL	**EXP$_{Cl\ Br\ I}$**	**CTRL**	**EXP$_{Cl\ Br\ I}$**
O_x Formation: $F(O_x)$				
RO_2 + NO	2.16	2.21	0.20	0.21
HO_2 + NO	2.05	2.09	0.39	0.34
Total $F(O_x)$	4.21	4.30	0.58	0.55
O_x Destruction: $D(O_x)$				
NO_2 loss[1]	0.33	0.35	0.05	0.04
NO_3 loss[2]	0.17	0.09	< 0.01	< 0.01
N_2O_5 loss[3]	0.20	0.12	0.03	0.02
O_3 loss[4]	0.26	0.24	0.13	0.12
O^{1D} loss[5]	0.16	0.17	0.18	0.17
Halogen loss[6]	0	0.01	0	0.12
Total $D(O_x)$	1.12	0.97	0.38	0.48
Total O_x production: $P(O_x)$				
$P(O_x)$ = $F(O_x)$ - $D(O_x)$	3.08	3.33	0.21	0.07

NO_2 loss[1]= NO_2+RO_2 and NO_2+OH
NO_3 loss[2]= NO_3+VOC
N_2O_5 loss[3]= Heterogeneous reaction of N_2O_5
O_3 loss[4]= O_3 + OH, O_3 + VOC, and O_3 + HO_2
O^{1D} loss[5]= O^{1D}+H_2O
Halogen loss[6]= XO + O_3, HO_2, and O^{3p}; ClO + NO_2; XO + XO (where X denotes Cl, Br, and I)
Halogen loss[6]= ClO + O_3, NO_2, and O^{3p}; Cl + O_3; BrO + OH; XO + HO_2; XO + XO (where X denotes Cl, Br, and I)

3.3 Impacts of halogen chemistry on atmospheric species

Figure 9~~8~~ summarizes the impacts of halogen processes on the mixing ratios of key

atmospheric species over/around the Korean peninsula. The mixing ratios of hydroxyl radicals

(OH) and hydroperoxyl radicals (HO_2) increased by ~0.002 ppt (2.2%) and ~0.13 ppt (1.6%),

respectively, when including the chlorine processes (i.e., EXP_{Cl} - CTRL). This is due to the

fact that the chlorine radicals in the atmosphere substitute the role of OH radicals. In other

words, chlorine radicals actively react with VOCs. Thus, the VOC mixing ratios decreased by

0.39 ppb (1.0%) due to the active VOC oxidation by Cl radicals. Formaldehyde (HCHO), an

intermediate product of VOC oxidation, increased by 0.02 ppb (1.1%) due to the enhanced

647 rates of the VOC oxidations by Cl radicals. The NO_x mixing ratios also increased by ~0.26 ppb

648 (2.6%). Higher levels of NO_x may be due to the elevated levels of $ClNO_2$, which is a precursor

649 of NO_x in the atmosphere.

650 　　　　We also explored the impacts of bromine processes (i.e., EXP_{Cl_Br} − EXP_{Cl}). The

651 mixing ratios of OH, HO_2, and HCHO further increased by ~0.001 ppt (1.1%), ~0.03 ppt (0.4%),

652 and ~0.01 ppb (0.5%), respectively. These patterns appear to be similar to those in the chlorine

653 case.

654 　　　　The effects of iodine chemistry (i.e., $EXP_{Cl\_Br\_I}$ − EXP_{Cl_Br}) revealed that OH mixing

655 ratios increased by 0.004 ppt (3.1%). However, the mixing ratios of HO_2 decreased by 0.32 ppt

656 (3.8%). Interestingly, this increase in OH contrasts with a previous global-scale study (e.g., Li

657 et al., 2022), where iodine chemistry typically leads to lower OH due to halogen-driven O_3

658 suppression and reduced $O(^1D)$ production. This discrepancy can likely be attributed to

659 differences in the spatial and temporal scales of the analysis. Specifically, our study focuses on

660 a short-term episode (i.e., the KORUS-AQ campaign), during which OH mixing ratios may be

661 more strongly influenced by halogen-mediated radical regeneration. For instance, reactions

662 such as $IO + HO_2 \rightarrow HOI$, followed by HOI photolysis ($HOI \xrightarrow{h\nu} I + OH$), can provide an

663 additional OH source that partially compensate for the O_3-related OH loss. Similar findings

664 have been reported in previous studies (Saiz-Lopez et al., 2012; Mahajan et al., 2021; Stone et

665 al., 2018). This may be due to the complicated interactions of the following reactions: (i) IO +

666 O₃ → IO; (ii) IO + HO₂ → HOI; (iii) HOI $\xrightarrow{h\nu}$ I + OH (null cycle: O₃ + HO₂ → 2OH + O₂).

667 Such patterns are prevalent over remote ocean areas affected by iodine chemistry. The levels

668 of HCHO and VOCs remain almost unchanged due to the fact that iodine radicals do not

669 strongly participate in the reactions with VOCs. The NO_x levels increased slightly by ~0.03

41

ppb (0.3%) on land and decreased by ~0.03 ppb (4.8%) over ocean areas, which is in line with

findings from the previous study (Mahajan et al., 2021).

Collectively, the influence of the full halogen ~~chemistries~~ chemistry (i.e., $EXP_{Cl\_Br\_I}$ −

CTRL) shows that the OH mixing ratios increased significantly by 0.007 ppt (5.5%), while the

HO_2 mixing ratios decreased by 0.45 ppt (5.~~4~~3%) over ocean areas. These patterns are

comparable in magnitude to those reported in previous studies. For example, Stone et al. (2018)

reported a 2% increase in OH and a 5% decrease in HO_2. In addition, Sarwar et al. (2015) found

a slight decrease in OH (1%) accompanied by a more pronounced decrease in HO_2 (11%).~~quite~~

~~similar to those observed in the GEOS-Chem modeling study (Stone et al., 2018).~~ The mixing

ratios of HCHO and NO_x increased by ~0.03 ppb (1.6%) and ~0.29 ppb (2.9%) over the land.

On the contrary, the mixing ratios of VOCs and NO_x decreased by ~0.71 ppb (5.9%) and ~0.05

ppb (7.8%) over the ocean areas, respectively. The reduction in NO_x over ocean is consistent

with Wang et al. (2021), who reported a similar decrease of approximately 6% due to halogen

chemistry.

In addition, elevated oxidant capacity in the simulation of $EXP_{Cl\_Br\_I}$ results in

enhancements in the concentrations of sulfate by 0.05 $\mu g \cdot m^{-3}$ (1.5%) and secondary organic

aerosols by 0.14 $\mu g \cdot m^{-3}$ (1.8%). However, concentrations of nitrate and ammonium decreased

by ~1.60 $\mu g \cdot m^{-3}$ (29.4%) and ~0.55 $\mu g \cdot m^{-3}$ (5.0%), respectively, as shown in Fig. S6. This

resulted from using smaller uptake coefficient for N_2O_5 (refer to Fig. S3), which suppresses

NH_4NO_3 formation. As a result, $PM_{2.5}$ levels decreased from 21.59 $\mu g \cdot m^{-3}$ to 20.63 $\mu g \cdot m^{-3}$

(10.5%) over the Korean Peninsula during the KORUS-AQ campaign.

691

692

43
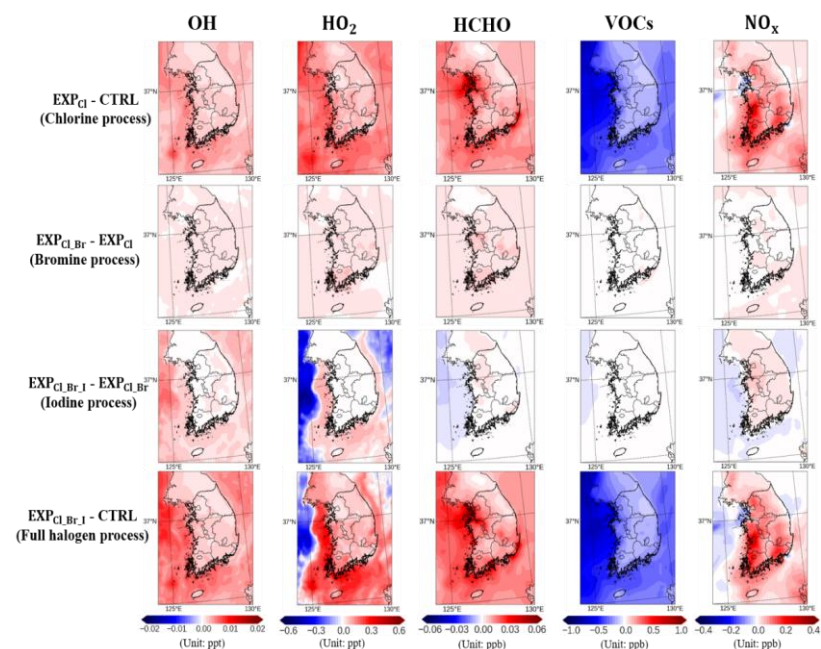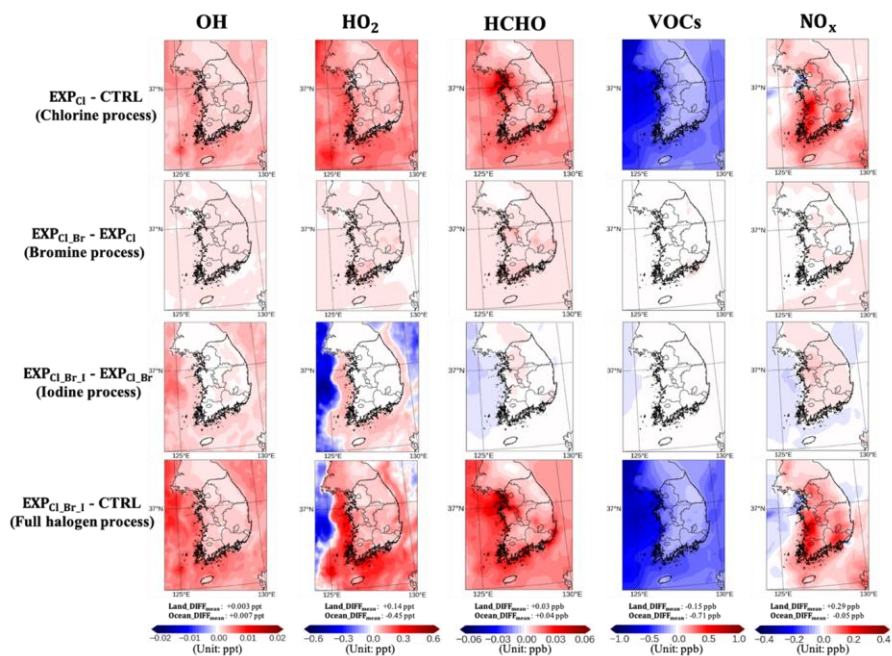
Figure 8~~9~~. Summaries of the impacts of chlorine processes (EXP$_{Cl}$ – CTRL), bromine processes (EXP$_{Cl\_Br}$ – EXP$_{Cl}$), iodine processes (EXP$_{Cl\_Br\_I}$ – EXP$_{Cl\_Br}$), and full halogen processes (EXP$_{Cl\_Br\_I}$ – CTRL) on the mixing ratios of OH, HO$_2$, HCHO, VOCs, and NO$_x$, respectively, during the period of KORUS-AQ campaign. Also, Land_DIFF$_{mean}$ and Ocean_DIFF$_{mean}$ indicate the differences in the averaged mixing ratios of each species between EXP$_{Cl\_Br\_I}$ and CTRL simulations, over land and ocean, respectively.

4. Summary and Conclusions

To investigate the impacts of halogen chemistry over the Korean peninsula, we attempted to add and update reactions involving three halogen species (Cl, Br, and I) in the CMAQ modeling system. ~~incorporate the halogen processes into the CMAQ modeling system.~~ First, we estimated anthropogenic emissions of HCl, Cl$_2$, HBr, and Br$_2$ from five main sectors (such as industry, residential areas, power plants, solid waste incineration, and others). The anthropogenic emissions for HCl, Cl$_2$, HBr, and Br$_2$ ~~are~~ were estimated to be 5,989.6, 450.8, 460.8, and 240.8 Mg·yr^{-1} over our research domain, respectively. Second, we also estimated emissions of natural halocarbons and inorganic bromine and iodine (Br$_2$, I$_2$~~I~~, and HOI), based on the information derived from the GOCI sensor. Finally, we embedded halogen chemical reactions (58 chlorine reactions, 64 bromine reactions, and 55 iodine reactions) into the CMAQ model.

We then tested the model performances in terms of the mixing ratios of ClNO$_2$ during the period of the KORUS-AQ campaign at two supersites in South Korea. The EXP$_{Cl\_Br\_I}$ simulation exhibited the best performance in terms of the mixing ratios of ClNO$_2$. With the EXP$_{Cl\_Br\_I}$ simulation, the IOA increased from 0.41 to 0.66 at the Olympic Park station, and 0.40 to 0.59 at the Mt. Taehwa station. Meanwhile, the MB decreased from -85.97 ppt to 30.79 ppt at the Olympic Park station, and -159.36 ppt to -25.07 ppt at the Mt. Taehwa station. This is because the four following halogen reactions considered in this study contributed to better ClNO$_2$ simulations: (i) ClO + ClO $\rightarrow$ Cl$_2$; (ii) HOBr + Cl$^-$ $\rightarrow$ BrCl; (iii) different parameterization of γ_{N2O5}; and (iv) 2NO$_2$ + Cl$^-$ $\rightarrow$ ClNO + NO$_3^-$.

44

In addition to the evaluation of $ClNO_2$, we assessed the overall performance of the implemented halogen chemistry by comparing simulated BrO and IO mixing ratios with previously reported observational and modeling results. The simulated mixing ratios of BrO and IO fall within the reported ranges of $0.0 - 1.3$ ppt for BrO and $0.0 - 2.5$ ppt for IO. This indicates that the updated halogen processes can reasonably reproduce the regional-scale behavior of bromine and iodine species.

Our study further emphasized the significant influences of individual halogen processes on O_3 mixing ratios over South Korea. The average mixing ratios of O_3 increased by ~ 0.21 ppb (0.5%) over land areas due to the impacts of chlorine and bromine processes. On the contrary, the O_3 mixing ratios decreased by ~ 0.69 ppb (1.2%) over ocean areas due to iodine processes. In addition, we quantitatively calculated the O_x budget. The net O_x production rate $(P(O_x))$ increased from 3.08 to 3.323 ppb/h over the land areas and decreased from 0.21 to 0.07 ppb/h over the ocean areas with the simulation of the $EXP_{Cl\_Br\_I}$.

Finally, we further explored the impacts of full halogen processes on the atmospheric composition. Compared with the CTRL simulation, the mixing ratios of HCHO and NO_x increased by ~ 0.03 ppb (1.6%) and ~ 0.29 ppb (2.9%) over the land, respectively. On the other hand, the mixing ratios of HO_2 and VOCs decreased by ~ 0.45 ppt (5.3%) and ~ 0.71 ppb (5.9%) over the ocean areas, respectively, during the period of the KORUS-AQ campaign.

In conclusion, we believe that we successfully incorporated comprehensive halogen processes into the CMAQ modeling system. Although our evaluation was limited to a few halogen-containing species, the developed framework allowed us to explore the broader impact of halogen chemistry on atmospheric composition and air quality. Despite these contributions, several limitations in modeling fields remain, including (i) the spatiotemporal variability of halogen emissions, (ii) incomplete or uncertain chemical mechanisms, and (iii) limited observational data. In this context, further research is needed to better understand and reduce

45

746   these uncertainties. ~~Although our study showed good agreement with observations, this is only~~

747   ~~in terms of a few species such as ClNO$_2$ and Cl$_2$. There are still lack of information such as~~

748   ~~insufficient observational data, uncertainties in uptake coefficients of reactive halogen species,~~

749   ~~and uncertainties in the reaction rates of these species. Obviously, further studies are necessary~~

750   ~~in the future to investigate these uncertainties in the halogen chemistry.~~

Code and data availability

Author contributions
Conceptualization: KK, CHS, and KMH. Writing: KK, CHS, and KMH. Experimental design: KK, CHS, KMH, GY, and RB. Supervision: CHS. Validation: KK and CHS. Analysis: KK. Data curation: SK. All authors contributed to this paper for publication.

Competing interests
At least one of the (co-)authors is a member of the editorial board of *Atmospheric Chemistry and Physics*. The authors declare that they have no known competing financial interests or personal relationships that could have appeared to influence the work reported in this paper.

Acknowledgment

References

Abbatt, J. and Waschewsky, G.: Heterogeneous interactions of HOBr, HNO3, O3, and NO2 with deliquescent NaCl aerosols at room temperature, J. Phys. Chem. A, 102, 3719-3725, https://doi.org/10.1021/jp980932d, 1998.

Allan, B. J., McFiggans, G., Plane, J. M., and Coe, H.: Observations of iodine monoxide in the remote marine boundary layer, J. Geophys. Res., 105, 14363-14369, https://doi.org/10.1029/1999JD901188, 2000.

Ammann, M., Cox, R. A., Crowley, J., Jenkin, M. E., Mellouki, A., Rossi, M. J., Troe, J., and Wallington, T. J.: Evaluated kinetic and photochemical data for atmospheric chemistry: Volume VI–heterogeneous reactions with liquid substrates, Atmos. Chem. Phys., 13, 8045-8228, https://doi.org/10.5194/acp-13-8045-2013, 2013.

Badia, A., Reeves, C. E., Baker, A. R., Saiz-Lopez, A., Volkamer, R., Koenig, T. K., Apel, E. C., Hornbrook, R. S., Carpenter, L. J., and Andrews, S. J.: Importance of reactive halogens in the tropical marine atmosphere: a regional modelling study using WRF-Chem, Atmos. Chem. Phys., 19, 3161-3189, https://doi.org/10.5194/acp-19-3161-2019, 2019.

Baklanov, A., Chesnokov, E., and Chichinin, A.: Rate constants for the reactions of molecular iodine with Cl, SiCl3, and SiH3 at 298 K, International Journal of Chemical Kinetics, 29, 25-33, https://doi.org/10.1002/(SICI)1097-4601(1997)29:1<25::AID-KIN4>3.0.CO;2-N, 1997.

Bedjanian, Y., Le Bras, G., and Poulet, G.: Rate constants for the reactions I+ OClO, I+ ClO, Cl+ I2, and Cl+ IO and heat of formation of IO radicals, J. Phys. Chem., 100, 15130-15136, https://doi.org/10.1021/jp960696b, 1996.

Bertram, T. and Thornton, J.: Toward a general parameterization of N2O5 reactivity on aqueous particles: the competing effects of particle liquid water, nitrate and chloride, Atmos. Chem. Phys., 9, 8351-8363, https://doi.org/10.5194/acp-9-8351-2009, 2009.

Burkholder, J., Sander, S., Abbatt, J., Barker, J., Cappa, C., Crounse, J., Dibble, T., Huie, R., Kolb, C., and Kurylo, M.: Chemical kinetics and photochemical data for use in atmospheric studies; evaluation number 19, Nasa panel for data evaluation technical report, 19-5, https://jpldataeval.jpl.nasa.gov/pdf/NASA-JPL%20Evaluation%2019-5.pdf, 2020.

Byun, D. and Schere, K. L.: Review of the governing equations, computational algorithms, and other components of the Models-3 Community Multiscale Air Quality (CMAQ) modeling system, Appl. Mech. Rev., 59, 51-77, https://doi.org/10.1115/1.2128636, 2006.

Caram, C., Szopa, S., Cozic, A., Bekki, S., Cuevas, C. A., and Saiz-Lopez, A.: Sensitivity of tropospheric ozone to halogen chemistry in the chemistry–climate model LMDZ-INCA vNMHC, Geosci. Model Dev., 16, 4041-4062, https://doi.org/10.5194/gmd-16-4041-2023, 2023.

Carter, W. P.: Development of the SAPRC-07 chemical mechanism, Atmos. Environ., 44, 5324-5335, https://doi.org/10.1016/j.atmosenv.2010.01.026, 2010.

Chang, W. L., Brown, S. S., Stutz, J., Middlebrook, A. M., Bahreini, R., Wagner, N. L., Dubé, W. P., Pollack, I. B., Ryerson, T. B., and Riemer, N.: Evaluating N2O5 heterogeneous hydrolysis parameterizations for CalNex 2010, J. Geophys. Res., 121, 5051-5070, https://doi.org/10.1002/2015JD024737, 2016.

Chen, H., Liu, P., Wang, Q., Huang, R., and Sarwar, G.: Impact and pathway of halogens on atmospheric oxidants in coastal city clusters in the Yangtze River Delta region in China, Atmospheric pollution research, 15, 101979, https://doi.org/10.1016/j.apr.2023.101979, 2024.

Chen, Q., Xia, M., Peng, X., Yu, C., Sun, P., Li, Y., Liu, Y., Xu, Z., Xu, Z., and Wu, R.: Large daytime molecular chlorine missing source at a suburban site in East China, J. Geophys. Res., 127, e2021JD035796, https://doi.org/10.1029/2021JD035796, 2022.

Clyne, M. and Cruse, H.: Atomic resonance fluorescence spectrometry for rate constants of rapid bimolecular reactions. Part 1.—Reactions O+ NO 2, Cl+ ClNO, Br+ ClNO, J. Chem. Soc. Faraday Trans., 68, 1281-1299, https://doi.org/10.1039/F29726801281, 1972.

Crawford, J. H., Ahn, J.-Y., Al-Saadi, J., Chang, L., Emmons, L. K., Kim, J., Lee, G., Park, J.-H., Park, R. J., and Woo, J. H.: The Korea–United States air quality (KORUS-AQ) field study, Elem Sci Anth, 9, 00163, https://doi.org/10.1525/elementa.2020.00163, 2021.

Deiber, G., George, C., Le Calvé, S., Schweitzer, F., and Mirabel, P.: Uptake study of ClONO 2 and BrONO 2 by Halide containing droplets, Atmos. Chem. Phys., 4, 1291-1299, https://doi.org/10.5194/acp-4-1291-2004, 2004.

Deng, S., Shi, Y., Liu, Y., Zhang, C., Wang, X., Cao, Q., Li, S., and Zhang, F.: Emission characteristics of Cd, Pb and Mn from coal combustion: Field study at coal-fired power plants in China, Fuel Processing Technology, 126, 469-475, https://doi.org/10.1016/j.fuproc.2014.06.009, 2014.

Edwards, P. M. and Young, C. J.: Primary Radical Effectiveness: Do the Different Chemical Reactivities of Hydroxyl and Chlorine Radicals Matter for Tropospheric Oxidation?, ACS ES&T Air, https://doi.org/10.1021/acsestair.3c00108, 2024.

829   Evans, M. J. and Jacob, D. J.: Impact of new laboratory studies of N2O5 hydrolysis on global model budgets of
830   tropospheric nitrogen oxides, ozone, and OH, Geophys. Res. Lett., 32, https://doi.org/10.1029/2005GL022469,
831   2005.
832   Fan, S. and Li, Y.: The impacts of marine-emitted halogens on OH radicals in East Asia during summer, Atmos.
833   Chem. Phys., 22, 7331-7351, https://doi.org/10.5194/acp-22-7331-2022, 2022.
834   Fernandez, R. P., Salawitch, R., Kinnison, D. E., Lamarque, J.-F., and Saiz-Lopez, A.: Bromine partitioning in the
835   tropical tropopause layer: implications for stratospheric injection, Atmos. Chem. Phys., 14, 13391-13410,
836   https://doi.org/10.5194/acp-14-13391-2014, 2014.
837   Gantt, B., Sarwar, G., Xing, J., Simon, H., Schwede, D., Hutzell, W. T., Mathur, R., and Saiz-Lopez, A.: The
838   impact of iodide-mediated ozone deposition and halogen chemistry on surface ozone concentrations across
839   the continental United States, Environ. Sci. Technol., 51, 1458-1466, https://doi.org/10.1021/acs.est.6b03556,
840   2017.
841   Giri, B. R., Farooq, A., Szőri, M., and Roscoe, J. M.: The kinetics of the reactions of Br atoms with the xylenes:
842   an   experimental   and   theoretical   study,   Phys.   Chem.   Chem.   Phys.,   24,   4843-4858,
843   https://doi.org/10.1039/D1CP03740D, 2022.
844   Großmann, K., Frieß, U., Peters, E., Wittrock, F., Lampel, J., Yilmaz, S., Tschritter, J., Sommariva, R., Von Glasow,
845   R., and Quack, B.: Iodine monoxide in the Western Pacific marine boundary layer, Atmos. Chem. Phys., 13,
846   3363-3378, https://doi.org/10.5194/acp-13-3363-2013, 2013.
847   Guenther, A., Jiang, X., Heald, C. L., Sakulyanontvittaya, T., Duhl, T. a., Emmons, L., and Wang, X.: The Model
848   of Emissions of Gases and Aerosols from Nature version 2.1 (MEGAN2. 1): an extended and updated
849   framework for modeling biogenic emissions, Geosci. Model Dev., 5, 1471-1492, https://doi.org/10.5194/gmd-
850   5-1471-2012, 2012.
851   Herrmann, M., Schöne, M., Borger, C., Warnach, S., Wagner, T., Platt, U., and Gutheil, E.: Ozone depletion events
852   in the Arctic spring of 2019: a new modeling approach to bromine emissions, Atmos. Chem. Phys., 22, 13495-
853   13526, https://doi.org/10.5194/acp-22-13495-2022, 2022.
854   Huang, Y., Lu, X., Fung, J. C., Sarwar, G., Li, Z., Li, Q., Saiz-Lopez, A., and Lau, A. K.: Effect of bromine and
855   iodine chemistry on tropospheric ozone over Asia-Pacific using the CMAQ model, Chemosphere, 262, 127595,
856   https://doi.org/10.1016/j.chemosphere.2020.127595, 2021.
857   Hutzell, W., Luecken, D., Appel, K., and Carter, W.: Interpreting predictions from the SAPRC07 mechanism based
858   on   regional   and   continental   simulations,   Atmos.   Environ.,   46,   417-429,
859   https://doi.org/10.1016/j.atmosenv.2011.09.030, 2012.
860   Iglesias-Suarez, F., Badia, A., Fernandez, R. P., Cuevas, C. A., Kinnison, D. E., Tilmes, S., Lamarque, J.-F., Long,
861   M. C., Hossaini, R., and Saiz-Lopez, A.: Natural halogens buffer tropospheric ozone in a changing climate,
862   Nature Climate Change, 10, 147-154, https://doi.org/10.1038/s41558-019-0675-6, 2020.
863   Jeong, D., Seco, R., Gu, D., Lee, Y., Nault, B. A., Knote, C. J., Mcgee, T., Sullivan, J. T., Jimenez, J. L., and
864   Campuzano-Jost, P.: Integration of airborne and ground observations of nitryl chloride in the Seoul
865   metropolitan area and the implications on regional oxidation capacity during KORUS-AQ 2016, Atmos. Chem.
866   Phys., 19, 12779-12795, https://doi.org/10.5194/acp-19-12779-2019, 2019.
867   Jiang, J., Hao, J., Wu, Y., Streets, D. G., Duan, L., and Tian, H.: Development of mercury emission inventory from
868   coal combustion in China, Environ. Sci., 26, 34-39, https://doi.org/10.13227/j.hjkx.2005.02.007, 2005 (in
869   Chinese).
870   Jo, H.-Y., Park, J., Heo, G., Lee, H.-J., Jeon, W., Kim, J.-M., Kim, S., Kim, J.-K., Liu, Y., and Liu, P.: Interpretation
871   of the effects of anthropogenic chlorine on nitrate formation over northeast Asia during KORUS-AQ 2016,
872   Sci. Total Environ., 164920, https://doi.org/10.1016/j.scitotenv.2023.164920, 2023.
873   Keefer, R. and Andrews, L.: The interaction of bromine with benzene and certain of its derivatives, J. Am. Chem.
874   Soc., 72, 4677-4681, https://doi.org/10.1021/ja01166a091, 1950.
875   Khamaganov, V. and Crowley, J.: Rate coefficients for the reactions CH3+ Br2 (224–358 K), CH3CO+ Br2 (228
876   and 298 K), and Cl+ Br2 (228 and 298 K), International Journal of Chemical Kinetics, 42, 575-585,
877   https://doi.org/10.1002/kin.20505, 2010.
878   Kim, H., Park, R. J., Kim, S., Jeong, J. I., Jeong, D., Fu, X., and Cho, S.: Effect of nitryl chloride chemistry on air
879   quality   in   South   Korea   during   the   KORUS-AQ   campaign,   Atmos.   Environ.,   312,   120045,
880   https://doi.org/10.1016/j.atmosenv.2023.120045, 2023.
881   Kim, W., Moon, J.-E., Park, Y.-J., and Ishizaka, J.: Evaluation of chlorophyll retrievals from Geostationary Ocean
882   color imager (GOCI) for the north-east Asian region, Remote Sens. Environ., 184, 482-495,
883   https://doi.org/10.1016/j.rse.2016.07.031, 2016.
884   Koenig, T. K., Volkamer, R., Baidar, S., Dix, B., Wang, S., Anderson, D. C., Salawitch, R. J., Wales, P. A., Cuevas,
885   C. A., and Fernandez, R. P.: BrO and inferred Br y profiles over the western Pacific: relevance of inorganic
886   bromine sources and a Br y minimum in the aged tropical tropopause layer, Atmos. Chem. Phys., 17, 15245-
887   15270, https://doi.org/10.5194/acp-17-15245-2017, 2017.

Le Breton, M., Bannan, T. J., Shallcross, D. E., Khan, M. A., Evans, M. J., Lee, J., Lidster, R., Andrews, S., Carpenter, L. J., and Schmidt, J.: Enhanced ozone loss by active inorganic bromine chemistry in the tropical troposphere, Atmos. Environ., 155, 21-28, https://doi.org/10.1016/j.atmosenv.2017.02.003, 2017.

Li, Q., Borge, R., Sarwar, G., de la Paz, D., Gantt, B., Domingo, J., Cuevas, C. A., and Saiz-Lopez, A.: Impact of halogen chemistry on summertime air quality in coastal and continental Europe: application of the CMAQ model and implications for regulation, Atmos. Chem. Phys., 19, 15321-15337, https://doi.org/10.5194/acp-19-15321-2019, 2019.

Li, Q., Zhang, L., Wang, T., Tham, Y. J., Ahmadov, R., Xue, L., Zhang, Q., and Zheng, J.: Impacts of heterogeneous uptake of dinitrogen pentoxide and chlorine activation on ozone and reactive nitrogen partitioning: improvement and application of the WRF-Chem model in southern China, Atmos. Chem. Phys., 16, 14875-14890, https://doi.org/10.5194/acp-16-14875-2016, 2016.

Li, Q., Fernandez, R. P., Hossaini, R., Iglesias-Suarez, F., Cuevas, C. A., Apel, E. C., Kinnison, D. E., Lamarque, J.-F., and Saiz-Lopez, A.: Reactive halogens increase the global methane lifetime and radiative forcing in the 21st century, Nat. Commun., 13, 2768, https://doi.org/10.1038/s41467-022-30456-8, 2022.

Li, Q., Badia, A., Wang, T., Sarwar, G., Fu, X., Zhang, L., Zhang, Q., Fung, J., Cuevas, C. A., and Wang, S.: Potential effect of halogens on atmospheric oxidation and air quality in China, J. Geophys. Res., 125, e2019JD032058, https://doi.org/10.1029/2019JD032058, 2020.

Li, Q., Fu, X., Peng, X., Wang, W., Badia, A., Fernandez, R. P., Cuevas, C. A., Mu, Y., Chen, J., and Jimenez, J. L.: Halogens enhance haze pollution in China, Environ. Sci. Technol., 55, 13625-13637, https://doi.org/10.1021/acs.est.1c01949, 2021.

Liss, P. S., Marandino, C. A., Dahl, E. E., Helmig, D., Hintsa, E. J., Hughes, C., Johnson, M. T., Moore, R. M., Plane, J. M., and Quack, B.: Short-lived trace gases in the surface ocean and the atmosphere, Ocean-atmosphere Interactions of Gases and Particles, 1-54, https://doi.org/10.1007/978-3-642-25643-1_1, 2014.

Liu, L., Bei, N., Wu, J., Liu, S., Zhou, J., Li, X., Yang, Q., Feng, T., Cao, J., and Tie, X.: Effects of stabilized Criegee intermediates (sCIs) on sulfate formation: a sensitivity analysis during summertime in Beijing–Tianjin–Hebei (BTH), China, Atmos. Chem. Phys., 19, 13341-13354, https://doi.org/10.5194/acp-19-13341-2019, 2019.

Liu, T. and Abbatt, J. P.: An experimental assessment of the importance of S (IV) oxidation by hypohalous acids in the marine atmosphere, Geophys. Res. Lett., 47, e2019GL086465, https://doi.org/10.1029/2019GL086465, 2020.

Liu, Y., Fan, Q., Chen, X., Zhao, J., Ling, Z., Hong, Y., Li, W., Chen, X., Wang, M., and Wei, X.: Modeling the impact of chlorine emissions from coal combustion and prescribed waste incineration on tropospheric ozone formation in China, Atmos. Chem. Phys., 18, 2709-2724, https://doi.org/10.5194/acp-18-2709-2018, 2018.

Mahajan, A. S., Li, Q., Inamdar, S., Ram, K., Badia, A., and Saiz-Lopez, A.: Modelling the impacts of iodine chemistry on the northern Indian Ocean marine boundary layer, Atmos. Chem. Phys., 21, 8437-8454, https://doi.org/10.5194/acp-21-8437-2021, 2021.

Mahajan, A. S., Plane, J., Oetjen, H., Mendes, L., Saunders, R., Saiz-Lopez, A., Jones, C., Carpenter, L., and McFiggans, G.: Measurement and modelling of tropospheric reactive halogen species over the tropical Atlantic Ocean, Atmos. Chem. Phys., 10, 4611-4624, https://doi.org/doi/10.5194/acp-10-4611-2010, 2010.

Mahajan, A. S., Gómez Martín, J. C., Hay, T. D., Royer, S. J., Yvon-Lewis, S., Liu, Y., Hu, L., Prados-Roman, C., Ordóñez, C., Plane, J. M. C., and Saiz-Lopez, A.: Latitudinal distribution of reactive iodine in the Eastern Pacific and its link to open ocean sources, Atmos. Chem. Phys., 12, 11609-11617, https://doi.org/10.5194/acp-12-11609-2012, 2012.

McDuffie, E. E., Fibiger, D. L., Dubé, W. P., Lopez-Hilfiker, F., Lee, B. H., Thornton, J. A., Shah, V., Jaeglé, L., Guo, H., and Weber, R. J.: Heterogeneous N2O5 uptake during winter: Aircraft measurements during the 2015 WINTER campaign and critical evaluation of current parameterizations, J. Geophys. Res., 123, 4345-4372, https://doi.org/10.1002/2018JD028336, 2018.

O'Reilly, J. E. and Werdell, P. J.: Chlorophyll algorithms for ocean color sensors-OC4, OC5 & OC6, Remote Sens. Environ., 229, 32-47, https://doi.org/10.1016/j.rse.2019.04.021, 2019.

Park, M.-O., Shin, W.-C., Son, Y.-B., and Noh, T.-G.: Spatial Variability of in situ and GOCI and MODIS Chlorophyll and CDOM in Summer at the East Sea, Journal of the Korean Society of Marine Environment & Safety, 21, 327-338, https://doi.org/10.7837/kosomes.2015.21.4.327, 2015.

Parrella, J., Jacob, D. J., Liang, Q., Zhang, Y., Mickley, L. J., Miller, B., Evans, M., Yang, X., Pyle, J., and Theys, N.: Tropospheric bromine chemistry: implications for present and pre-industrial ozone and mercury, Atmos. Chem. Phys., 12, 6723-6740, https://doi.org/10.5194/acp-12-6723-2012, 2012.

PENG, B.-x. and WU, D.-s.: Distribution and content of bromine in Chinese coals, Journal of Fuel Chemistry and Technology, 42, 769-773, https://doi.org/10.1016/S1872-5813(14)60034-7, 2014.

Peng, X., Wang, T., Wang, W., Ravishankara, A., George, C., Xia, M., Cai, M., Li, Q., Salvador, C. M., and Lau,

947   C.: Photodissociation of particulate nitrate as a source of daytime tropospheric Cl2, Nat. Commun., 13, 939,
948   https://doi.org/10.6084/m9.figshare.17099252, 2022.
949   Peters, C., Pechtl, S., Stutz, J., Hebestreit, K., Hönninger, G., Heumann, K., Schwarz, A., Winterlik, J., and Platt,
950   U.: Reactive and organic halogen species in three different European coastal environments, Atmos. Chem.
951   Phys., 5, 3357-3375, https://doi.org/10.5194/acp-5-3357-2005, 2005.
952   Prados-Román, C., Cuevas, C. A., Hay, T., Fernández, R. P., Mahajan, A. S., Royer, S.-J., Galí, M., Simó, R.,
953   Dachs, J., and Großmann, K.: Iodine oxide in the global marine boundary layer, Atmos. Chem. Phys., 15, 583-
954   593, https://doi.org/10.5194/acp-15-583-2015, 2015.
955   Pratte, P. and Rossi, M. J.: The heterogeneous kinetics of HOBr and HOCl on acidified sea salt and model aerosol
956   at 40–90% relative humidity and ambient temperature, Phys. Chem. Chem. Phys., 8, 3988-4001,
957   https://doi.org/10.1039/B604321F, 2006.
958   Qiu, X., Ying, Q., Wang, S., Duan, L., Wang, Y., Lu, K., Wang, P., Xing, J., Zheng, M., and Zhao, M.: Significant
959   impact of heterogeneous reactions of reactive chlorine species on summertime atmospheric ozone and free-
960   radical formation in north China, Sci. Total Environ., 693, 133580,
961   https://doi.org/10.1016/j.scitotenv.2019.133580, 2019a.
962   Qiu, X., Ying, Q., Wang, S., Duan, L., Zhao, J., Xing, J., Ding, D., Sun, Y., Liu, B., and Shi, A.: Modeling the
963   impact of heterogeneous reactions of chlorine on summertime nitrate formation in Beijing, China, Atmos.
964   Chem. Phys., 19, 6737-6747, https://doi.org/10.5194/acp-19-6737-2019, 2019b.
965   Read, K. A., Mahajan, A. S., Carpenter, L. J., Evans, M. J., Faria, B. V., Heard, D. E., Hopkins, J. R., Lee, J. D.,
966   Moller, S. J., and Lewis, A. C.: Extensive halogen-mediated ozone destruction over the tropical Atlantic Ocean,
967   Nature, 453, 1232-1235, https://doi.org/10.1038/nature07035, 2008.
968   Riedel, T., Bertram, T., Ryder, O., Liu, S., Day, D., Russell, L., Gaston, C., Prather, K., and Thornton, J.: Direct
969   N 2 O 5 reactivity measurements at a polluted coastal site, Atmos. Chem. Phys., 12, 2959-2968,
970   https://doi.org/10.5194/acp-12-2959-2012, 2012a.
971   Riedel, T. P., Bertram, T. H., Crisp, T. A., Williams, E. J., Lerner, B. M., Vlasenko, A., Li, S.-M., Gilman, J., De
972   Gouw, J., and Bon, D. M.: Nitryl chloride and molecular chlorine in the coastal marine boundary layer, Environ.
973   Sci. Technol., 46, 10463-10470, https://doi.org/10.1021/es204632r, 2012b.
974   Riemer, N., Vogel, H., Vogel, B., Schell, B., Ackermann, I., Kessler, C., and Hass, H.: Impact of the heterogeneous
975   hydrolysis of N2O5 on chemistry and nitrate aerosol formation in the lower troposphere under photosmog
976   conditions, J. Geophys. Res.-Atmos., 108, https://doi.org/10.1029/2002JD002436, 2003.
977   Roberts, J. M., Osthoff, H. D., Brown, S. S., Ravishankara, A., Coffman, D., Quinn, P., and Bates, T.: Laboratory
978   studies of products of N2O5 uptake on Cl− containing substrates, Geophys. Res. Lett., 36,
979   https://doi.org/10.1029/2009GL040448, 2009.
980   Saiz-Lopez, A., Fernandez, R. P., Ordóñez, C., Kinnison, D. E., Gómez Martín, J., Lamarque, J.-F., and Tilmes,
981   S.: Iodine chemistry in the troposphere and its effect on ozone, Atmos. Chem. Phys., 14, 13119-13143,
982   https://doi.org/10.5194/acp-14-13119-2014, 2014.
983   Saiz-Lopez, A., Fernandez, R. P., Li, Q., Cuevas, C. A., Fu, X., Kinnison, D. E., Tilmes, S., Mahajan, A. S., Gómez
984   Martín, J. C., and Iglesias-Suarez, F.: Natural short-lived halogens exert an indirect cooling effect on climate,
985   Nature, 618, 967-973, https://doi.org/10.1038/s41586-023-06119-z, 2023.
986   Saiz-Lopez, A., Lamarque, J.-F., Kinnison, D. E., Tilmes, S., Ordóñez, C., Orlando, J. J., Conley, A. J., Plane, J.,
987   Mahajan, A. S., and Sousa Santos, G.: Estimating the climate significance of halogen-driven ozone loss in the
988   tropical marine troposphere, Atmos. Chem. Phys., 12, 3939-3949, https://doi.org/10.5194/acp-12-3939-2012,
989   2012.
990   Sander, S., Friedl, R., Golden, D., Kurylo, M., Moortgat, G., Wine, P., Ravishankara, A., Kolb, C., Molina, M.,
991   and Finlayson-Pitts, B.: Chemical kinetics and photochemical data for use in atmospheric studies: Evaluation
992   number 15, Pasadena, CA: Jet Propulsion Laboratory, California Institute of Technology2010.
993   Sarwar, G., Simon, H., Bhave, P., and Yarwood, G.: Examining the impact of heterogeneous nitryl chloride
994   production on air quality across the United States, Atmos. Chem. Phys., 12, 6455-6473,
995   https://doi.org/10.5194/acp-12-6455-2012, 2012.
996   Sarwar, G., Gantt, B., Schwede, D., Foley, K., Mathur, R., and Saiz-Lopez, A.: Impact of enhanced ozone
997   deposition and halogen chemistry on tropospheric ozone over the Northern Hemisphere, Environ. Sci.
998   Technol., 49, 9203-9211, https://doi.org/10.1021/acs.est.5b01657, 2015.
999   Sarwar, G., Gantt, B., Foley, K., Fahey, K., Spero, T. L., Kang, D., Mathur, R., Foroutan, H., Xing, J., and Sherwen,
1000 T.: Influence of bromine and iodine chemistry on annual, seasonal, diurnal, and background ozone: CMAQ
1001 simulations over the Northern Hemisphere, Atmos. Environ., 213, 395-404,
1002 https://doi.org/10.1016/j.atmosenv.2019.06.020, 2019.
1003 Sherwen, T., Evans, M., Carpenter, L., Andrews, S., Lidster, R., Dix, B., Koenig, T., Sinreich, R., Ortega, I., and
1004 Volkamer, R.: Iodine's impact on tropospheric oxidants: a global model study in GEOS-Chem, Atmos. Chem.
1005 Phys., 16, 1161-1186, https://doi.org/10.5194/acp-16-1161-2016, 2016.

Simpson, W. R., Brown, S. S., Saiz-Lopez, A., Thornton, J. A., and von Glasow, R.: Tropospheric halogen chemistry: Sources, cycling, and impacts, Chem. Rev., 115, 4035-4062, https://doi.org/10.1021/cr5006638, 2015.

Skamarock, W. C., Klemp, J. B., Dudhia, J., Gill, D. O., Barker, D. M., Duda, M. G., Huang, X.-Y., Wang, W., and Powers, J. G.: A description of the advanced research WRF version 3, NCAR technical note, 475, 10.5065, https://doi.org/10.5065/D68S4MVH, 2008.

Slusher, D. L., Huey, L. G., Tanner, D. J., Flocke, F. M., and Roberts, J. M.: A thermal dissociation–chemical ionization mass spectrometry (TD-CIMS) technique for the simultaneous measurement of peroxyacyl nitrates and dinitrogen pentoxide, J. Geophys. Res., 109, https://doi.org/10.1029/2004JD004670, 2004.

Son, H.-J.: Long-term variations of phytoplankton biomass and water quality in the downstream of Nakdong River, Journal of Korean Society of Environmental Engineers, 35, 263-267, https://doi.org/10.4491/KSEE.2024.46.11.687, 2013.

Stone, D., Sherwen, T., Evans, M. J., Vaughan, S., Ingham, T., Whalley, L. K., Edwards, P. M., Read, K. A., Lee, J. D., and Moller, S. J.: Impacts of bromine and iodine chemistry on tropospheric OH and HO 2: comparing observations with box and global model perspectives, Atmos. Chem. Phys., 18, 3541-3561, https://doi.org/10.5194/acp-18-3541-2018, 2018.

Takashima, H., Kanaya, Y., Kato, S., Friedrich, M. M., Van Roozendael, M., Taketani, F., Miyakawa, T., Komazaki, Y., Cuevas, C. A., and Saiz-Lopez, A.: Full latitudinal marine atmospheric measurements of iodine monoxide, Atmospheric Chemistry and Physics Discussions, 2021, 1-24, https://doi.org/10.5194/acp-22-4005-2022, 2021.

von Glasow, R. and Crutzen, P. J.: Tropospheric halogen chemistry, Treatise on Geochemistry, 4, 347, 2003.

Wang, X., Jacob, D. J., Downs, W., Zhai, S., Zhu, L., Shah, V., Holmes, C. D., Sherwen, T., Alexander, B., and Evans, M. J.: Global tropospheric halogen (Cl, Br, I) chemistry and its impact on oxidants, Atmos. Chem. Phys., 21, 13973-13996, https://doi.org/10.5194/acp-21-13973-2021, 2021.

Wang, X., Wang, H., Xue, L., Wang, T., Wang, L., Gu, R., Wang, W., Tham, Y. J., Wang, Z., and Yang, L.: Observations of N2O5 and ClNO2 at a polluted urban surface site in North China: High N2O5 uptake coefficients and low ClNO2 product yields, Atmos. Environ., 156, 125-134, https://doi.org/10.1016/j.atmosenv.2017.02.035, 2017.

Wiedinmyer, C., Akagi, S., Yokelson, R. J., Emmons, L., Al-Saadi, J., Orlando, J., and Soja, A.: The Fire INventory from NCAR (FINN): A high resolution global model to estimate the emissions from open burning, Geosci. Model Dev., 4, 625-641, https://doi.org/10.5194/gmd-4-625-2011, 2011.

Woo, J.-H., Kim, Y., Kim, H.-K., Choi, K.-C., Eum, J.-H., Lee, J.-B., Lim, J.-H., Kim, J., and Seong, M.: Development of the CREATE inventory in support of integrated climate and air quality modeling for Asia, Sustainability, 12, 7930, https://doi.org/10.3390/su12197930, 2020.

Yi, X., Yin, S., Huang, L., Li, H., Wang, Y., Wang, Q., Chan, A., Traoré, D., Ooi, M. C. G., and Chen, Y.: Anthropogenic emissions of atomic chlorine precursors in the Yangtze River Delta region, China, Sci. Total Environ., 771, 144644, https://doi.org/10.1016/j.scitotenv.2020.144644, 2021.

Yu, C., Wang, Z., Xia, M., Fu, X., Wang, W., Tham, Y. J., Chen, T., Zheng, P., Li, H., and Shan, Y.: Heterogeneous N2O5 reactions on atmospheric aerosols at four Chinese sites: improving model representation of uptake parameters, Atmos. Chem. Phys., 20, 4367-4378, https://doi.org/10.5194/acp-20-4367-2020, 2020.

Zhu, L., Jacob, D. J., Eastham, S. D., Sulprizio, M. P., Wang, X., Sherwen, T., Evans, M. J., Chen, Q., Alexander, B., and Koenig, T. K.: Effect of sea salt aerosol on tropospheric bromine chemistry, Atmos. Chem. Phys., 19, 6497-6507, https://doi.org/10.5194/acp-19-6497-2019, 2019.